SIAM J. SCI. COMPUT.
Vol. 42, No. 2, pp. B520–B547

UNIFORMLY ACCURATE METHODS FOR THREE DIMENSIONAL VLASOV EQUATIONS UNDER STRONG MAGNETIC FIELD WITH VARYING DIRECTION*

PHILIPPE CHARTIER†, NICOLAS CROUSEILLES†, MOHAMMED LEMOU†, FLORIAN MÉHATS†, AND XIAOFEI ZHAO‡

Abstract. In this paper, we consider the three dimensional Vlasov equation with an inhomogeneous, varying direction, strong magnetic field. Whenever the magnetic field has constant intensity, the oscillations generated by the stiff term are periodic. The homogenized model is then derived, and several state-of-the-art multiscale methods, in combination with the particle-in-cell discretization, are proposed for solving the Vlasov–Poisson equation. Their accuracy as much as their computational cost remain essentially independent of the strength of the magnetic field. The proposed schemes thus allow large computational steps, while the full gyro-motion can be restored by a linear interpolation in time. In the linear case, extensions are introduced for a general magnetic field (varying intensity and direction). Eventually, numerical experiments are exposed to illustrate the efficiency of the methods and some long-term simulations are presented.

Key words. Vlasov–Poisson equation, three dimensions, strong magnetic field, varying direction, uniformly accurate method, particle-in-cell

AMS subject classifications. 65L05, 65L20, 65L70

DOI. 10.1137/19M127402X

1. Introduction.

Vlasov models have been widely considered for modeling the dynamics of plasmas as encountered in magnetic fusion devices known as a tokamaks, where a strong external magnetic field is applied so as to confine the charged particles. In this paper, we consider the three dimensional Vlasov–Poisson equation with a strong nonhomogeneous magnetic field whose direction may vary [17, 25, 36]:

$$\partial_t f^\varepsilon(t,\mathbf{x},\mathbf{v}) + \mathbf{v}\cdot\nabla_{\mathbf{x}} f^\varepsilon(t,\mathbf{x},\mathbf{v}) + \left(\mathbf{E}(t,\mathbf{x}) + \frac{1}{\varepsilon}\mathbf{v}\times\mathbf{B}(\mathbf{x})\right)\cdot\nabla_{\mathbf{v}} f^\varepsilon(t,\mathbf{x},\mathbf{v}) = 0, \tag{1.1a}$$

$$\nabla_{\mathbf{x}}\cdot\mathbf{E}(t,\mathbf{x}) = \int_{\mathbb{R}^3} f^\varepsilon(t,\mathbf{x},\mathbf{v})d\mathbf{v} - n_i, \tag{1.1b}$$

$$f^\varepsilon(0,\mathbf{x},\mathbf{v}) = f_0(\mathbf{x},\mathbf{v}), \tag{1.1c}$$

*Submitted to the journal's Computational Methods in Science and Engineering section July 10, 2019; accepted for publication (in revised form) February 18, 2020; published electronically April 22, 2020.

https://doi.org/10.1137/19M127402X

Funding: This work was supported by the French ANR project MOONRISE ANR-14-CE23-0007-01. The fifth author's work was partially supported by the Natural Science Foundation of Hubei Province 2019CFA007 and by the NSFC through grant 11901440. This work was carried out within the framework of the French Federation for Magnetic Fusion Studies (FR-FCM) and of the Eurofusion consortium under grant agreement 633053.

†Univ Rennes, INRIA-MINGuS, CNRS, IRMAR-UMR 6625, F-35000 Rennes, France (Philippe.Chartier@inria.fr, nicolas.crouseilles@inria.fr, mohammed.lemou@univ-rennes1.fr, florian.mehats@univ-rennes1.fr).

‡Corresponding author. School of Mathematics and Statistics & Hubei Key Laboratory of Computational Science, Wuhan University, Wuhan, 430072, China, and Univ Rennes, INRIA-MINGuS, CNRS, IRMAR-UMR 6625, F-35000 Rennes, France (matzhxf@whu.edu.cn).

where, for a given $T > 0$,

$$f^\varepsilon : (t, \mathbf{x}, \mathbf{v}) \in [0, T] \times \mathbb{R}^3 \times \mathbb{R}^3 \mapsto f^\varepsilon(t, \mathbf{x}, \mathbf{v}) \in \mathbb{R}$$

is the unknown,

$$f_0 : (\mathbf{x}, \mathbf{v}) \in \mathbb{R}^3 \times \mathbb{R}^3 \mapsto f_0(\mathbf{x}, \mathbf{v}) \in \mathbb{R}$$

a given initial distribution, where

$$\mathbf{B} : \mathbf{x} \in \mathbb{R}^3 \mapsto \mathbf{B}(\mathbf{x}) \in \mathbb{R}^3$$

denotes the external magnetic field,

$$\mathbf{E} : (t, \mathbf{x}) \in \mathbb{R}^+ \times \mathbb{R}^3 \mapsto \mathbf{E}(t, \mathbf{x}) \in \mathbb{R}^3$$

the self-consistent electric-field function, $0 < \varepsilon \leq 1$ a dimensionless parameter inversely proportional to the strength of the magnetic field, and $n_i \geq 0$ the ion density of the background. The system (1.1) has a lot of invariants, and we will be interested in particular in the Hamiltonian defined by

$$\mathcal{H}(t) := \int_{\mathbb{R}^3} \int_{\mathbb{R}^3} \frac{1}{2} |\mathbf{v}|^2 f^\varepsilon(t, \mathbf{x}, \mathbf{v}) d\mathbf{x} d\mathbf{v} + \frac{1}{2} \int_{\mathbb{R}^3} |\mathbf{E}(t, \mathbf{x})|^2 d\mathbf{x}. \tag{1.2}$$

The above Vlasov–Poisson model (1.1) is derived from the three dimensional Vlasov–Maxwell equations by considering the electrostatic approximation. Unlike some asymptotically reduced models, such as the gyrokinetic equations [30, 34] or the drift-kinetic limit equations [3, 24, 19], model (1.1) contains the information from the angle variable and it is of paramount importance for studying the plasma dynamics in the tokamak device.

In the strong magnetic field limit regime, the charged particles exhibit very fast rotations with the cyclotron period proportional to ε, while remaining confined along the magnetic line. In such a case, the small parameter $0 < \varepsilon \ll 1$ renders the solution $f^\varepsilon(t, \mathbf{x}, \mathbf{v})$ of (1.1) highly oscillatory in time. Classical numerical integrators such as splitting or finite-difference schemes thus require time steps smaller than the cyclotron period in order to accurately capture the dynamics, thus implying severe computational burden. Recent efforts have aimed at designing numerical schemes which allow step sizes much larger than the cyclotron period. Upon assuming that the magnetic field has a fixed direction in space, i.e., that

$$\mathbf{B}(\mathbf{x}) = (0, 0, b(\mathbf{x}))^T, \quad b(\mathbf{x}) > 0$$

(a popular choice both for formal and rigorous analyses [3, 17, 25]), several multiscale numerical methods have been proposed [8, 16, 18, 20, 21, 22]. Among them, Filbet et al. constructed particle-in-cell (PIC) schemes in the spirit of asymptotic preserving techniques [28], which, as $\varepsilon \to 0$, are consistent with the drift-limit model [20] or the gyrokinetic model [18, 21]. These schemes are simple and highly accurate, but the gyro-motion is lost in the limit regime. In contrast, the schemes proposed in [8, 16] capture all the information of the kinetic models with an accuracy uniform with respect to $0 < \varepsilon \leq 1$. These *uniformly accurate (UA)* schemes have computational cost as well as accuracy totally independent of ε (we refer the reader to [13] for a comparison of UA scheme with other multiscale methods). In order to design UA schemes for kinetic models, different numerical approaches may be used: (i) The two-scale formulation technique relies upon an explicit separation of the fast and slow times

and allows one to smooth out the oscillations [8, 15, 16]. (ii) The multi-revolution composition methods, in the spirit of the heterogeneous multiscale method [1], are also UA, as confirmed in the recent paper [9]. Both approaches exploit the periodicity of the solution of the stiff part of the equation. For instance, our recent work [8] isolates the dominant oscillation frequency owing to a confining property in two dimensions. However, the general case of a strong magnetic field with varying direction, i.e.,

$$\mathbf{B}(\mathbf{x}) = (b_1(\mathbf{x}), b_2(\mathbf{x}), b_3(\mathbf{x}))^T,$$

has been barely considered so far for the Vlasov–Poisson equation (1.1) due to its complicated highly oscillatory behavior in three dimensions. Let us also mention recent developments around the symplectic PIC method, which allows for good preservation of invariants for very long times (see [26, 33, 29]).

In this work, we propose efficient numerical schemes for solving the three dimensional Vlasov–Poisson equation (1.1) in the strong magnetic field regime by combining multiscale strategies with the PIC discretization. First, we consider the case of a magnetic field with constant intensity $|\mathbf{B}(\mathbf{x})| = \text{const}$, for which, as already pointed out in [6, 34], the motion induced by the stiff Lorentz term $\frac{1}{\varepsilon}\mathbf{v} \times \mathbf{B}(\mathbf{x})$ in (1.1) is periodic in time. Taking advantage of this observation, we derive the limit model of (1.1) by using averaging methods [6] and then introduce three UA schemes, namely (i) the multi-revolution composition (MRC) method, (ii) the two-scale formulation (TSF) method, and (iii) the micro-macro (MM) method. All three are of uniform second order in time for all $\varepsilon \in]0, 1]$, but they have specific pros and cons: for instance, MRC methods are phase-space volume preserving, while MM easily allows for the full recovery of the gyro-motion. To the best of our knowledge, this key feature is new and paves the way for an extension to the case of a magnetic field with varying intensity. In this situation, we indeed introduce, under the PIC discretization, a reparametrization of time to renormalize the magnetic field. Within this framework, each particle carries its own fictitious time. Hence, and in order to avoid the occurrence of multiple frequencies, we drop in this situation the Poisson part of (1.1) and consider instead the case of an external electric field $\mathbf{E}(t, \mathbf{x})$ (this somehow simplifying assumption is relevant, as it marks an important first step towards the solution of the full problem). In order to resynchronize all particles (a necessary step in order to provide an approximation of $f^\varepsilon(t, \mathbf{x}, \mathbf{v})$), we then use the interpolation strategy of MM which ensures uniform second order except for the angular variable. Eventually, numerical experiments are presented in order to validate uniform accuracy and to compare the various methods. In particular, we simulate the dynamics of (1.1) in a three dimensional screw-pinch setup [30].

The remainder of the paper is now organized as follows. Section 2 considers the limit model of (1.1) with a constant intensity $\mathbf{B}(\mathbf{x})$, and section 3 introduces the three aforementioned UA schemes in this situation: Subsection 3.1 is concerned with the MRC method, subsection 3.2 with the TSF method, and subsection 3.3 with the MM method. Extensions to the case of a varying intensity are presented in section 4. Finally, numerical results with concluding remarks are shown in section 5.

2. Averaging. A general assumption throughout this paper is that the magnetic field is bounded from below, i.e., that $|\mathbf{B}(\mathbf{x})| \geq c_0$ for all $\mathbf{x} \in \mathbb{R}^3$ for some $c_0 > 0$ independent of ε. In this section, we further assume that the external magnetic field has constant norm

$$|\mathbf{B}(\mathbf{x})| \equiv \text{const} > 0, \quad \mathbf{x} \in \mathbb{R}^3,$$

so that the stiff part of (1.1) generates periodic motion. This setup was also studied in [25]. A viable case of such a $\mathbf{B}$ is given by $\mathbf{B}(\mathbf{x}) = (B_1(x_1, x_2), B_2(x_1, x_2), B_3(x_1, x_2))$, where

$$B_3 = \sqrt{\|B_1^2 + B_2^2\|_{L^\infty(\mathbb{R}^2)} - B_1^2 - B_2^2},$$

with $(B_1(x_1, x_2), B_2(x_1, x_2)) \in L^\infty(\mathbb{R}^2)$ and $\partial_{x_1} B_1 + \partial_{x_2} B_2 = 0$. It can be verified that $|\mathbf{B}(\mathbf{x})|^2 \equiv \|B_1^2 + B_2^2\|_{L^\infty(\mathbb{R}^2)}$ and $\nabla_x \cdot \mathbf{B} \equiv 0$. In such a case, we are able to apply a recently developed averaging method to quickly obtain the limit model of (1.1) as $\varepsilon \to 0$.

LEMMA 2.1. *If $|\mathbf{B}(\mathbf{x})| \equiv b$ for some constant $b > 0$, then the solution of*

$$\partial_t \tilde{f}^\varepsilon(t, \mathbf{x}, \mathbf{v}) + \frac{1}{\varepsilon} \mathbf{v} \times \mathbf{B}(\mathbf{x}) \cdot \nabla_{\mathbf{v}} \tilde{f}^\varepsilon(t, \mathbf{x}, \mathbf{v}) = 0 \tag{2.1}$$

is $2\pi/b$-periodic with respect to the fast time-variable t/ε.

Proof. The characteristics of (2.1)

$$\dot{\mathbf{x}}(t) = 0, \quad \dot{\mathbf{v}}(t) = \frac{1}{\varepsilon} \mathbf{v}(t) \times \mathbf{B}(\mathbf{x}(t)), \quad t > 0,$$

have a periodic solution in t/ε which can be obtained, for instance, by the Rodrigues formula

(2.2)
$$\begin{aligned} &\mathbf{x}(t) = \mathbf{x}(0), \\ &\mathbf{v}(t) = \cos(bt/\varepsilon)\mathbf{v}(0) + (1 - \cos(bt/\varepsilon))(\mathbf{B}(\mathbf{x}(0)) \cdot \mathbf{v}(0))\mathbf{B}(\mathbf{x}(0)) + \sin(bt/\varepsilon)\mathbf{v}(0) \times \mathbf{B}(\mathbf{x}(0)). \end{aligned}$$

The statement of the lemma is now an immediate consequence. ∎

Using the observation above, we may apply the following theorem from [6].

THEOREM 2.2. *Consider a transport equation of the form*

$$\partial_t f^\varepsilon(t, \mathbf{y}) + \left[\frac{G(\mathbf{y})}{\varepsilon} + K(\mathbf{y}) \right] \cdot \nabla_{\mathbf{y}} f^\varepsilon(t, \mathbf{y}) = 0, \quad f^\varepsilon(0, \mathbf{y}) = f_0(\mathbf{y}),$$

where the flow map Φ_t of

$$\dot{\mathbf{y}}(t) = G(\mathbf{y}(t))$$

is assumed to be 2π-periodic. There exist two formal *vector fields $G^\varepsilon(\mathbf{y})$ and $K^\varepsilon(\mathbf{y})$ satisfying*

$$\frac{G(\mathbf{y})}{\varepsilon} + K(\mathbf{y}) = \frac{G^\varepsilon(\mathbf{y})}{\varepsilon} + K^\varepsilon(\mathbf{y}) \quad \text{and} \quad [G^\varepsilon, K^\varepsilon] := \partial_{\mathbf{y}} G^\varepsilon K^\varepsilon - \partial_{\mathbf{y}} K^\varepsilon G^\varepsilon = 0,$$

such that the system

$$\begin{cases} \partial_\tau g(t, \tau, \mathbf{y}) + G^\varepsilon(\mathbf{y}) \cdot \nabla_{\mathbf{y}} g(t, \tau, \mathbf{y}) = 0, & \text{(2.3a)} \\ \partial_t g(t, \tau, \mathbf{y}) + K^\varepsilon(\mathbf{y}) \cdot \nabla_{\mathbf{y}} g(t, \tau, \mathbf{y}) = 0, & \text{(2.3b)} \\ g(0, 0, \mathbf{y}) = f_0(\mathbf{y}) & \text{(2.3c)} \end{cases}$$

has a unique formal solution independently of the order in which the equations are solved. Moreover, for all positive time we have $f^\varepsilon(t, \mathbf{y}) = g(t, t/\varepsilon, \mathbf{y})$ and the first two terms of $K^\varepsilon = K^{[1]} + \varepsilon K^{[2]} + O(\varepsilon^2)$ may be computed as follows:

$$K^{[1]} = \Pi K_\tau, \quad K^{[2]} = -\frac{1}{2} \Pi \int_0^\tau [K_s, K_\tau] ds, \quad \text{with} \quad K_\tau(\mathbf{y}) := (D_{\mathbf{y}} \Phi_\tau(\mathbf{y}))^{-1} (K \circ \Phi_\tau)(\mathbf{y}),$$

with $\Pi h := 1/(2\pi) \int_0^{2\pi} h(\tau) d\tau$.

Remark 2.3. If K^ε is truncated at order k in ε and $G^\varepsilon = G(y) + \varepsilon K(y) - \varepsilon K^\varepsilon$, then the order in which the equations in (2.3) are solved does matter. However, the difference between the corresponding two solutions is also of order ε^k.

Without loss of generality, we assume in the rest of this section that $|\mathbf{B}(\mathbf{x})| \equiv 1$ to derive the averaged model of (1.1) as obtained from Theorem 2.2. Details of the derivation may be found in [6], and we thus content ourselves with a sketch of the computations: from (1.1), we have

$$G = \begin{pmatrix} \mathbf{0} \\ \mathbf{v} \times \mathbf{B} \end{pmatrix}, \quad K = \begin{pmatrix} \mathbf{v} \\ \mathbf{E} \end{pmatrix},$$

and the flow map generated by G is given by

$$\Phi_\tau(\mathbf{y}) = \begin{pmatrix} \mathbf{x} \\ \cos(\tau)\mathbf{v} + \sin(\tau)\mathbf{v} \times \mathbf{B} + (1 - \cos(\tau))(\mathbf{B} \cdot \mathbf{v})\mathbf{B} \end{pmatrix}, \quad \mathbf{y} = \begin{pmatrix} \mathbf{x} \\ \mathbf{v} \end{pmatrix}.$$

Then

$$D_{\mathbf{y}}\Phi_\tau(\mathbf{y}) = \begin{pmatrix} I_3 & \mathbf{0} \\ N_1 & N_2 \end{pmatrix},$$

where

$$\begin{aligned} N_1 &= \sin(\tau)\,(\mathbf{v} \times \nabla_{\mathbf{x}}\mathbf{B}) + (1 - \cos(\tau))[(\mathbf{B} \cdot \mathbf{v})\nabla_{\mathbf{x}}\mathbf{B} + \mathbf{B}(\mathbf{v}^T\nabla_{\mathbf{x}}\mathbf{B})], \\ N_2 &= \cos(\tau)I_3 - \sin(\tau)(\mathbf{B} \times I_3) + (1 - \cos(\tau))\mathbf{B}\mathbf{B}^T, \end{aligned}$$

where we have denoted $\mathbf{v} \times \nabla_{\mathbf{x}}\mathbf{B} = [\mathbf{v} \times \partial_{x_1}\mathbf{B}, \mathbf{v} \times \partial_{x_2}\mathbf{B}, \mathbf{v} \times \partial_{x_3}\mathbf{B}]$ and similarly for $\mathbf{v} \times I_3$. A straightforward calculation then leads to

$$\Pi\left((D_{\mathbf{y}}\Phi_\tau(\mathbf{y}))^{-1}(K \cdot \Phi_\tau)\right) = \begin{pmatrix} (\mathbf{B} \cdot \mathbf{v})\mathbf{B} \\ \mathbf{B}_{\mathbf{v}} \end{pmatrix},$$

where

$$\begin{aligned} \mathbf{B}_{\mathbf{v}} = \mathbf{B}\mathbf{B}^T &\left[\mathbf{E} - \frac{1}{2}(\mathbf{v} \times \nabla_{\mathbf{x}}\mathbf{B})(\mathbf{v} \times \mathbf{B}) + M\mathbf{v} - \frac{5}{2}M(\mathbf{B} \cdot \mathbf{v})\mathbf{B}\right] - \frac{1}{2}M\left[\mathbf{v} - 2(\mathbf{B} \cdot \mathbf{v})\mathbf{B}\right] \\ &- \frac{1}{2}\mathbf{B} \times I_3\left[M(\mathbf{v} \times \mathbf{B}) + (\mathbf{v} \times \nabla_{\mathbf{x}}\mathbf{B})(\mathbf{B} \cdot \mathbf{v})\mathbf{B}\right], \end{aligned}$$

with

$$M = (\mathbf{B} \cdot \mathbf{v})\nabla_{\mathbf{x}}\mathbf{B} + \mathbf{B}(\mathbf{v}^T\nabla_{\mathbf{x}}\mathbf{B}).$$

Eventually,

$$K^\varepsilon = \begin{pmatrix} (\mathbf{B} \cdot \mathbf{v})\mathbf{B} \\ \mathbf{B}_{\mathbf{v}} \end{pmatrix} + O(\varepsilon),$$

and the limit model at leading order is

$$\partial_t g(t, \tau, \mathbf{x}, \mathbf{v}) + (\mathbf{B} \cdot \mathbf{v})\mathbf{B} \cdot \nabla_{\mathbf{x}} g(t, \tau, \mathbf{x}, \mathbf{v}) + \mathbf{B}_{\mathbf{v}} \cdot \nabla_{\mathbf{v}} g(t, \tau, \mathbf{x}, \mathbf{v}) = 0, \quad t > 0.$$

By taking $\tau = 0$ and $f(t, \mathbf{x}, \mathbf{v}) = g(t, 0, \mathbf{x}, \mathbf{v})$, we get the leading order averaged model of (1.1) for stroboscopic times $t \in 2\pi\varepsilon\mathbb{N}$,

$$\partial_t f(t, \mathbf{x}, \mathbf{v}) + (\mathbf{B} \cdot \mathbf{v})\mathbf{B} \cdot \nabla_{\mathbf{x}} f(t, \mathbf{x}, \mathbf{v}) + \mathbf{B}_{\mathbf{v}} \cdot \nabla_{\mathbf{v}} f(t, \mathbf{x}, \mathbf{v}) = 0, \tag{2.4a}$$

$$\nabla_{\mathbf{x}} \cdot \mathbf{E}(t, \mathbf{x}) = \int_{\mathbb{R}^3} f(t, \mathbf{x}, \mathbf{v}) d\mathbf{v} - n_i, \tag{2.4b}$$

$$f(0, \mathbf{x}, \mathbf{v}) = f_0(\mathbf{x}, \mathbf{v}). \tag{2.4c}$$

As we shall verify later numerically, we have

$$f^\varepsilon(t,\mathbf{x},\mathbf{v}) - f(t,\mathbf{x},\mathbf{v}) = O(\varepsilon), \quad 0 < \varepsilon \ll 1, \quad t \in 2\pi\varepsilon\mathbb{N}.$$

Similar limit models including higher order corrections have been obtained in [4, 25] via different approaches.

3. Numerical method. In this section, we introduce numerical schemes for (1.1) under the assumption $|\mathbf{B}(\mathbf{x})| \equiv 1$. Taking advantage of the periodicity of the solution of the stiff part, we apply state-of-art multiscale approaches in combination with PIC discretization. In this way, we obtain schemes whose accuracy and computational cost are both independent of $\varepsilon \in]0,1]$. Our starting point is the following PIC representation of f^ε as used in, e.g., [20, 22, 27, 36]:

$$f^\varepsilon(t,\mathbf{x},\mathbf{v}) \approx \sum_{k=1}^{N_p} \omega_k \delta(\mathbf{x}-\mathbf{x}_k(t))\delta(\mathbf{v}-\mathbf{v}_k(t)), \quad t \geq 0,\ \mathbf{x},\mathbf{v} \in \mathbb{R}^2. \tag{3.1}$$

The characteristic equations of model (1.1) for $1 \leq k \leq N_p$ are then of the form

$$\dot{\mathbf{x}}_k(t) = \mathbf{v}_k(t), \tag{3.2a}$$

$$\dot{\mathbf{v}}_k(t) = \mathbf{E}(t,\mathbf{x}_k(t)) + \frac{1}{\varepsilon}\mathbf{v}_k(t) \times \mathbf{B}(\mathbf{x}_k(t)), \quad t > 0, \tag{3.2b}$$

$$\mathbf{x}_k(0) = \mathbf{x}_{k,0}, \quad \mathbf{v}_k(0) = \mathbf{v}_{k,0}. \tag{3.2c}$$

Noticing that

$$\nabla_{\mathbf{x}} \cdot \mathbf{E}(t,\mathbf{x}) = \sum_{k=1}^{N_p} w_k \delta(\mathbf{x}-\mathbf{x}_k(t)) - n_i,$$

we observe that the electric field $\mathbf{E}$ in (3.2) has in fact no explicit dependence on time, i.e., $\mathbf{E}(t,\mathbf{x}) = \mathbf{E}_{[X(t)]}(\mathbf{x})$, where $X(t) = (\mathbf{x}_1(t),\dots,\mathbf{x}_{N_p}(t))$. We are in a position to briefly present three different UA methods.

3.1. Multi-revolution composition method. For a general exposition of multi-revolution composition (MRC), we refer the reader to [11]. Here we focus on a uniformly accurate second order method.

MRC framework. Suppose that we wish to solve (1.1) on $[0,T_f]$ for some $T_f > 0$. Rescaling time in (3.2) leads to (we omit the particle index for brevity)

$$\dot{\mathbf{x}}(t) = \varepsilon\mathbf{v}(t), \tag{3.3a}$$

$$\dot{\mathbf{v}}(t) = \varepsilon\mathbf{E}_{[X(t)]}(\mathbf{x}(t)) + \mathbf{v}(t) \times \mathbf{B}(\mathbf{x}(t)), \quad 0 < t \leq \frac{T_f}{\varepsilon}, \tag{3.3b}$$

$$\mathbf{x}(0) = \mathbf{x}_0, \quad \mathbf{v}(0) = \mathbf{v}_0. \tag{3.3c}$$

Since the stiff part of (3.3) generates a 2π-periodic motion, (3.3) is amenable to MRC [11, 12]. To do so, we write

$$\frac{T_f}{\varepsilon} = 2\pi M_f + T_r, \quad M_f = \left\lfloor \frac{T_f}{2\pi\varepsilon} \right\rfloor \in \mathbb{N}, \quad 0 \leq T_r < 2\pi. \tag{3.4}$$

The second order MRC method begins by choosing an integer $0 < M_0 \leq M_f$ and defining

$$\alpha = \frac{1}{2}\left(1 + \frac{1}{M_0}\right), \quad \beta = \frac{1}{2}\left(1 - \frac{1}{M_0}\right), \quad M = \frac{M_f}{M_0}, \quad H = \varepsilon M_0. \tag{3.5}$$

Denoting $\mathbf{x}^n \approx \mathbf{x}(2\pi n M_0)$, $\mathbf{v}^n \approx \mathbf{v}(2\pi n M_0)$, the MRC scheme proceeds as follows:

$$\begin{pmatrix}\mathbf{x}^{n+1}\\ \mathbf{v}^{n+1}\end{pmatrix} = \mathcal{E}_\beta(-2\pi)\mathcal{E}_\alpha(2\pi)\begin{pmatrix}\mathbf{x}^{n}\\ \mathbf{v}^{n}\end{pmatrix}, \quad 0 \le n \le M-1, \tag{3.6}$$

where $\mathcal{E}_\alpha(2\pi)$ denotes the value at time 2π of the flow of

$$\begin{cases} \dot{\mathbf{x}}(t) = \alpha H \mathbf{v}(t), \\ \dot{\mathbf{v}}(t) = \alpha H \mathbf{E}_{[X(t)]}(\mathbf{x}(t)) + \mathbf{v}(t) \times \mathbf{B}(\mathbf{x}(t)) \end{cases} \tag{3.7}$$

and $\mathcal{E}_\beta(-2\pi)$ the value at time (-2π) of the flow of

$$\begin{cases} \dot{\mathbf{x}}(t) = -\beta H \mathbf{v}(t), \\ \dot{\mathbf{v}}(t) = -\beta H \mathbf{E}_{[X(t)]}(\mathbf{x}(t)) + \mathbf{v}(t) \times \mathbf{B}(\mathbf{x}(t)). \end{cases} \tag{3.8}$$

The solution at final time T_f is then obtained by applying to $\binom{\mathbf{x}^M}{\mathbf{v}^M}$ the flow $\mathcal{E}_r(T_r)$ at time T_r of

$$\begin{cases} \dot{\mathbf{x}}(t) = \varepsilon \mathbf{v}(t), \\ \dot{\mathbf{v}}(t) = \varepsilon \mathbf{E}_{[X(t)]}(\mathbf{x}(t)) + \mathbf{v}(t) \times \mathbf{B}(\mathbf{x}(t)). \end{cases} \tag{3.9}$$

Splitting scheme. The full MRC scheme calls for the numerical evaluation of the subflows $\mathcal{E}_\alpha(2\pi)$, $\mathcal{E}_\beta(2\pi)$, and $\mathcal{E}_r(T_r)$. This is done here through a splitting, for instance of $\mathcal{E}_\alpha$, in

$$\mathcal{E}^{\mathbf{x}}_\alpha(t): \begin{cases} \dot{\mathbf{x}}(s) = \alpha H \mathbf{v}(s), \\ \dot{\mathbf{v}}(s) = 0, \quad 0 < s \le t, \end{cases} \qquad \mathcal{E}^{\mathbf{v}}_\alpha(t): \begin{cases} \dot{\mathbf{x}}(s) = 0, \quad 0 < s \le t, \\ \dot{\mathbf{v}}(s) = \alpha H \mathbf{E}_{[X(s)]}(\mathbf{x}(s)) + \mathbf{v}(s) \times \mathbf{B}(\mathbf{x}(s)). \end{cases} \tag{3.10}$$

Note that both $\mathcal{E}^{\mathbf{x}}_\alpha(t)$ and $\mathcal{E}^{\mathbf{v}}_\alpha(t)$ can be exactly integrated. The exact flow of $\mathcal{E}^{\mathbf{x}}_\alpha(t)$ is clearly

$$\mathbf{x}(t) = \mathbf{x}(0) + t\alpha H \mathbf{v}(0), \quad \mathbf{v}(t) = \mathbf{v}(0), \quad t \ge 0,$$

while the exact flow of $\mathcal{E}^{\mathbf{v}}_\alpha(t)$, by using the Rodrigues rotation formula, can also be written explicitly as

$$\begin{aligned} \mathbf{x}(t) &= \mathbf{x}(0), \\ \mathbf{v}(t) &= \cos(t)\mathbf{v}(0) + \sin(t)\mathbf{v}(0) \times \mathbf{B} + \alpha H \sin(t)\mathbf{E} + \alpha H(t - \sin(t))(\mathbf{B} \cdot \mathbf{E})\mathbf{B} \\ &\quad + \alpha H(1 - \cos(t))\mathbf{E} \times \mathbf{B} \\ &\quad + (1 - \cos(t))(\mathbf{B} \cdot \mathbf{v}(0))\mathbf{B}, \quad t \ge 0, \end{aligned}$$

where $\mathbf{E} = \mathbf{E}_{[X(0)]}(\mathbf{x}(0))$ and $\mathbf{B} = \mathbf{B}(\mathbf{x}(0))$. In our experiments, we shall take the value of the (micro) time step $h = 2\pi/M$, so that

$$\mathcal{E}_\alpha(2\pi) \approx \left(\mathcal{E}^{\mathbf{x}}_\alpha(h/2)\mathcal{E}^{\mathbf{v}}_\alpha(h)\mathcal{E}^{\mathbf{x}}_\alpha(h/2)\right)^M.$$

Approximations for $\mathcal{E}_\beta(2\pi)$ and $\mathcal{E}_r(T_r)$ are obtained in a similar way. It may then be proved (see (3.6)) that the error of MRC is of size $O(M^{-2})$ for a computational cost of size M^2, making the overall scheme of order one.[1]

It remains to comment on what happens when the user-controlled M increases to the limit where M_0 reaches the critical value $M_0 = 1$, for which $\alpha = 1$, $\beta = 0$

[1] Under the assumption that $\mathbf{E}(t, \mathbf{x}) \in C^2(\mathbb{R}^+ \times \mathbb{R}^3; \mathbb{R}^3)$ and $\mathbf{B}(\mathbf{x}) \in C^2(\mathbb{R}^3; \mathbb{R}^3)$ in (3.2).

(3.5), and $\mathcal{E}_\beta(-2\pi) \equiv \mathrm{id}$. In this case, the full MRC scheme may be regarded as just the discretization of (3.3) by Strang's method with time step h. Therefore, as soon as $M > 0$ implies $M_0 = T_f/\varepsilon/(2\pi)/M < 1$, we replace the MRC method by Strang splitting with time step $h = 2\pi/M$. Finally, note that all vector fields involved in MRC are divergence-free so that their exact flows are *phase-space volume preserving*, as is the MRC method itself.

3.2. Two-scale formulation method. Two-scale formulation (TSF) methods have been developed in [7, 14]. Their underlying rationale is to consider the fast time as an additional variable. In order to isolate the fast time, we apply the change of unknowns $(\mathbf{x}(t), \mathbf{v}(t)) \mapsto (\mathbf{x}(t), \mathbf{y}(t))$, where

(3.11)
$$\mathbf{y}(t) = \cos(t/\varepsilon)\mathbf{v}(t) + (1-\cos(t/\varepsilon))(\mathbf{B}(\mathbf{x}(t))\cdot\mathbf{v}(t))\mathbf{B}(\mathbf{x}(t)) - \sin(t/\varepsilon)\mathbf{v}(t)\times\mathbf{B}(\mathbf{x}(t)).$$

This leads to

$$\begin{cases} \dot{\mathbf{x}}(t) = F_{\mathbf{x}}(t/\varepsilon, \mathbf{x}(t), \mathbf{y}(t)), \\ \dot{\mathbf{y}}(t) = F_{\mathbf{y}}(t/\varepsilon, \mathbf{x}(t), \mathbf{y}(t)), \quad t > 0, \\ \mathbf{x}(0) = \mathbf{x}_0, \quad \mathbf{y}(0) = \mathbf{v}_0, \end{cases} \tag{3.12}$$

where

$$F_{\mathbf{x}}(\tau, \mathbf{x}, \mathbf{y}) := \cos(\tau)\mathbf{y} + (1-\cos(\tau))(\mathbf{B}(\mathbf{x})\cdot\mathbf{y})\mathbf{B}(\mathbf{x}) + \sin(\tau)\mathbf{y}\times\mathbf{B}(\mathbf{x}),$$

and

$$\begin{aligned} F_{\mathbf{y}}(\tau, \mathbf{x}, \mathbf{y}) =& \cos(\tau)\mathbf{E}_{[X]}(\mathbf{x}) + (1-\cos(\tau))(\mathbf{B}(\mathbf{x})\cdot\mathbf{E}_{[X]}(\mathbf{x}))\mathbf{B}(\mathbf{x}) - \sin(\tau)\mathbf{E}_{[X]}(\mathbf{x})\times\mathbf{B}(\mathbf{x}) \\ &- \frac{1}{2}\sin(2\tau)\mathbf{q}_\tau(\mathbf{y}) - \frac{1}{2}(2\sin(\tau) - \sin(2\tau))\mathbf{q}_\tau((\mathbf{B}(\mathbf{x})\cdot\mathbf{y})\mathbf{B}(\mathbf{x})) \\ &- \frac{1}{2}(1-\cos(2\tau))\mathbf{q}_\tau(\mathbf{y}\times\mathbf{B}(\mathbf{x})) + \frac{1}{2}(2\cos(\tau) - \cos(2\tau) - 1)\mathbf{p}_\tau(\mathbf{y}) + \frac{1}{2}(3 - 4\cos(\tau) \\ &+ \cos(2\tau))\mathbf{p}_\tau((\mathbf{B}(\mathbf{x})\cdot\mathbf{y})\mathbf{B}(\mathbf{x})) + \frac{1}{2}(2\sin(\tau) - \sin(2\tau))\mathbf{p}_\tau(\mathbf{y}\times\mathbf{B}(\mathbf{x})), \end{aligned}$$

with the vector fields

$$\begin{aligned} \mathbf{p}_\tau(\mathbf{z}) &:= ((\nabla_{\mathbf{x}}\mathbf{B}(\mathbf{x})F_{\mathbf{x}}(\tau, \mathbf{x}, \mathbf{y}))\cdot\mathbf{z})\mathbf{B}(\mathbf{x}) + (\mathbf{B}(\mathbf{x})\cdot\mathbf{z})(\nabla_{\mathbf{x}}\mathbf{B}(\mathbf{x})F_{\mathbf{x}}(\tau, \mathbf{x}, \mathbf{y})), \\ \mathbf{q}_\tau(\mathbf{z}) &:= \mathbf{z}\times(\nabla_{\mathbf{x}}\mathbf{B}(\mathbf{x})F_{\mathbf{x}}(\tau, \mathbf{x}, \mathbf{y})), \quad \mathbf{z}\in\mathbb{R}^3. \end{aligned}$$

Denoting $\mathbf{u}(t) = \binom{\mathbf{x}(t)}{\mathbf{y}(t)}$ and $F(\tau, \mathbf{u}) = \binom{F_{\mathbf{x}}(\tau, \mathbf{x}, \mathbf{y})}{F_{\mathbf{y}}(\tau, \mathbf{x}, \mathbf{y})}$, the TSF of system (3.12) now reads as

$$\begin{aligned} &\partial_t U(t,\tau) + \frac{1}{\varepsilon}\partial_\tau U(t,\tau) = F(\tau, U(t,\tau)), \quad t > 0,\ \tau\in\mathbb{T}, \\ &U(0,0) = \mathbf{u}(0), \end{aligned} \tag{3.13}$$

where $\mathbb{T} = [0, 2\pi]$, and one recovers the solution of (3.12) by taking the diagonal, i.e.,

$$U(t, t/\varepsilon) = \mathbf{u}(t), \quad t \geq 0.$$

It remains to prescribe an appropriate initial datum $U(0,\tau)$ to (3.13) so that the solution U has its derivatives uniformly bounded up to some order.

Initial data. In order to derive $U(0,\tau)$, we follow the Chapman–Enskog procedure. From the decomposition

$$\underline{U}(t) = \Pi U(t,\cdot), \quad \mathbf{h}(t,\tau) = U(t,\tau) - \underline{U}(t), \ \text{ with } \Pi U(t,\cdot) = \frac{1}{2\pi}\int_0^{2\pi} U(t,\tau)d\tau,$$

we split (3.13) into

$$\begin{cases} \dot{\underline{U}}(t) = \Pi F(\cdot, \underline{U}(t) + \mathbf{h}(t,\cdot)), \quad t > 0, \\ \partial_t \mathbf{h}(t,\tau) + \dfrac{1}{\varepsilon}\partial_\tau \mathbf{h}(t,\tau) = (I-\Pi)F(\tau, \underline{U}(t) + \mathbf{h}(t,\tau)), \quad t > 0,\ \tau \in \mathbb{T}. \end{cases}$$

Denote $L = \partial_\tau$, $A = L^{-1}(I - \Pi)$, and we have

$$\mathbf{h}(t,\tau) = \varepsilon A F(\tau, \underline{U}(t) + \mathbf{h}(t,\tau)) - \varepsilon L^{-1}\partial_t \mathbf{h}(t,\tau).$$

Differentiate the above with respect to t on both sides:

$$\partial_t \mathbf{h}(t,\tau) = \varepsilon A \nabla F(\tau, \underline{U} + \mathbf{h})(\dot{\underline{U}} + \partial_t \mathbf{h}) - \varepsilon L^{-1}\partial_t^2 \mathbf{h}(t,\tau).$$

By assuming that $\partial_t^2 \mathbf{h} = O(1)$ for $\varepsilon \in]0,1]$, one gets $\partial_t \mathbf{h} = O(\varepsilon)$ and $\mathbf{h}(t,\tau)$ has the following first order asymptotic expansion:

$$\mathbf{h}(t,\tau) = \varepsilon A F(\tau, \underline{U}(t)) + O(\varepsilon^2).$$

Using the fact that $\underline{U}(0) = \mathbf{u}(0) - \mathbf{h}(0,0)$, one gets at initial time

$$\mathbf{h}(0,\tau) = \mathbf{h}^{1st}(\tau) + O(\varepsilon^2), \quad \text{with} \quad \mathbf{h}^{1st}(\tau) := \varepsilon A F(\tau, \mathbf{u}(0)),$$

and we denote the first order initial datum as

$$U^{1st}(\tau) := \mathbf{u}(0) + \mathbf{h}^{1st}(\tau) - \mathbf{h}^{1st}(0). \tag{3.14}$$

In fact, one can show rigorously that (3.13) with the well-prepared initial datum $U(0,\tau) = U^{1st}(\tau)$ offers

$$\partial_t U(t,\tau),\ \partial_t^2 U(t,\tau) = O(1), \quad \varepsilon \in]0,1]. \tag{3.15}$$

We refer the reader to [7] for the mathematical justification. The boundedness of the time derivatives (3.15) is the key to designing UA schemes.

Exponential integrator. Thanks to the TSF (3.13) with the well-prepared initial datum $U(0,\tau) = U^{1st}(\tau)$ from (3.14), we can now directly apply the second order exponential integrator scheme proposed in [16] for integrating (3.13): Choose $N_\tau > 0$ as an even integer to uniformly discretize τ on $\mathbb{T}$, and take a $\Delta t > 0$ to define $t_n = n\Delta t$. Denote $U^n(\tau) \approx U(t_n,\tau)$ for $n \geq 0$, and let $U^0(\tau) = U(0,\tau)$. We update the U^n for $n \geq 1$ as

$$\widehat{(U)}_l^{\,1} = \mathrm{e}^{-\frac{il\Delta t}{\varepsilon}}\widehat{(U)}_l^{\,0} + p_l\widehat{(F)}_l^{\,0} + q_l\frac{1}{\Delta t}\left(\widehat{(F)}_l^{\,*,1} - \widehat{(F)}_l^{\,0}\right), \tag{3.16a}$$

$$\widehat{(U)}_l^{\,n+1} = \mathrm{e}^{-\frac{il\Delta t}{\varepsilon}}\widehat{(U)}_l^{\,n} + p_l\widehat{(F)}_l^{\,n} + q_l\frac{1}{\Delta t}\left(\widehat{(F)}_l^{\,n} - \widehat{(F)}_l^{\,n-1}\right), \quad n \geq 1, \tag{3.16b}$$

where for $n \geq 0$,

$$U^n(\tau) = \sum_{l=-N_\tau/2}^{N_\tau/2-1} \widehat{(U)}_l^{\,n}\mathrm{e}^{il\tau}, \quad F^n(\tau) = \sum_{l=-N_\tau/2}^{N_\tau/2-1} \widehat{(F)}_l^{\,n}\mathrm{e}^{il\tau}, \quad F^{*,1}(\tau) = \sum_{l=-N_\tau/2}^{N_\tau/2-1} \widehat{(F)}_l^{\,*,1}\mathrm{e}^{il\tau},$$

and $F^n(\tau) = F(\tau, U^n(\tau))$, $F^{*,1}(\tau) = F(\tau, U^{*,1}(\tau))$, with

$$\widehat{(U)}_l^{\,*,1} = \mathrm{e}^{-\frac{il\Delta t}{\varepsilon}}\widehat{(U)}_l^{\,0} + p_l\widehat{(F)}_l^{\,0}, \quad U^{*,1}(\tau) = \sum_{l=-N_\tau/2}^{N_\tau/2-1} \widehat{(U)}_l^{\,*,1}\mathrm{e}^{il\tau}$$

and

$$p_l = \begin{cases} \dfrac{i\varepsilon}{l}\left(\mathrm{e}^{-\frac{il\Delta t}{\varepsilon}} - 1\right), & l \neq 0, \\ \Delta t, & l = 0, \end{cases} \qquad q_l = \begin{cases} \dfrac{\varepsilon}{l^2}\left(\varepsilon - \varepsilon \mathrm{e}^{-\frac{il\Delta t}{\varepsilon}} - il\Delta t\right), & l \neq 0, \\ \dfrac{\Delta t^2}{2}, & l = 0. \end{cases}$$

Suppose we have the numerical solution $U^n(\tau) = \binom{X^n(\tau)}{Y^n(\tau)}$ from the above scheme; then the numerical solution $\mathbf{x}^n \approx \mathbf{x}(t_n)$, $\mathbf{v}^n \approx \mathbf{v}(t_n)$ of the original characteristics (3.2) reads as

$$\begin{aligned} \mathbf{x}^n &= X^n(t_n/\varepsilon), \quad n \geq 1, \\ \mathbf{v}^n &= \cos(t_n/\varepsilon) Y^n(t_n/\varepsilon) \\ &\quad + (1 - \cos(t_n/\varepsilon))(\mathbf{B}(\mathbf{x}^n) \cdot Y^n(t_n/\varepsilon))\mathbf{B}(\mathbf{x}^n) \\ &\quad + \sin(t_n/\varepsilon) Y^n(t_n/\varepsilon) \times \mathbf{B}(\mathbf{x}^n). \end{aligned}$$

The derivation and convergence analysis of the above scheme can be found in [16]. Since the filter (3.11) involves the magnetic field $\mathbf{B}(\mathbf{x})$, the filtered system (3.12), which is less smooth than the original form (3.2), needs more regularity for optimal convergence of the algorithm. Assuming that $\mathbf{E}(t, \mathbf{x}) \in C^2(\mathbb{R}^+ \times \mathbb{R}^3; \mathbb{R}^3)$ and $\mathbf{B}(\mathbf{x}) \in C^3(\mathbb{R}^3; \mathbb{R}^3)$ in (3.2), the TSF exponential integrator (3.16) gives uniform second order accuracy in terms of Δt for all $\varepsilon \in]0, 1]$ and uniform spectral accuracy in terms of N_τ (due to periodicity):

$$O(\Delta t^2 + N_\tau^{-m_0}),$$

with $m_0 > 0$ arbitrarily large. The total cost of the TSF method is $O(\Delta t^{-1} N_\tau \log N_\tau)$.

3.3. Micro-macro method. Now we present the main new method of this work. It is based on the micro-macro (MM) decomposition that has been proposed very recently in [10]. We shall for the first time consider this approach for the Vlasov–Poisson equation and propose a second order UA scheme. The same notations will be adopted from the previous subsection.

MM decomposition. By the averaging theory [35], it is known that for general oscillatory problem

$$\dot{\mathbf{u}}(t) = F(t/\varepsilon, \mathbf{u}(t)), \quad t > 0, \tag{3.17}$$

with 2π-periodicity in τ of $F(\tau, \mathbf{u})$, the solution can be written as a composition

$$\mathbf{u}(t) = \Phi_{t/\varepsilon} \circ \Psi_t \circ \Phi_0^{-1}(\mathbf{u}(0)), \tag{3.18}$$

where $\Phi_\tau(\mathbf{v})$ is a change of variables with 2π-periodicity in τ for some $\mathbf{v}$, and $\Psi_t(\mathbf{v})$ is the flow map of the autonomous equation with initial value $\mathbf{v}$:

$$\dot{\Psi}_t(\mathbf{v}) = F_0(\Psi_t(\mathbf{v})), \quad \Psi_0(\mathbf{v}) = \mathbf{v} \tag{3.19}$$

for some field F_0. Though (3.18) is known to hold theoretically for some Φ_τ and Ψ_t, the explicit formulas of Φ_τ and Ψ_t are not available. In fact, by plugging (3.18) back into (3.17), the change of variables Φ_τ, the flow map Ψ_t, and the averaged field F_0 can be seen to satisfy the relation

$$\frac{1}{\varepsilon}\partial_\tau \Phi_\tau(\mathbf{v}) + D_{\mathbf{v}}\Phi_\tau(\mathbf{v}) F_0(\mathbf{v}) = F(\tau, \Phi_\tau(\mathbf{v})), \tag{3.20}$$

and, moreover, by taking averaging with respect to $\tau \in [0, 2\pi]$ on both sides of (3.20), one can define F_0 with Φ_τ,

$$F_0 = (\Pi D_{\mathbf{v}} \Phi_\tau)^{-1} \Pi F(\cdot, \Phi_\tau). \tag{3.21}$$

The above two equalities cannot completely determine Φ_τ and Ψ_t, so the standard averaging method imposes an extra condition $\Pi\Phi_\tau = \mathrm{id}$, which uniquely defines the change of variables Φ_τ in an implicit way through (3.20). In general, it is not possible to solve (3.20) to find out the exact Φ_τ. However, we can define an approximated Φ_τ through a kth order iteration

$$\Phi_\tau^{[k+1]} = \mathrm{id} + \varepsilon A \left(F(\tau, \Phi_\tau^{[k]}) - D_{\mathbf{v}} \Phi_\tau^{[k]} F_0^{[k]} \right), \quad k \in \mathbb{N}, \tag{3.22}$$

initially with

$$\Phi_\tau^{[0]} = \mathrm{id}, \quad F_0^{[0]} = \Pi F,$$

which asymptotically gives

$$\Phi_\tau = \Phi_\tau^{[k]} + O(\varepsilon^{k+1}).$$

Here the operator A is defined in the same way as in the previous subsection. As a compensation to the composition (3.18), by using the approximated function $\Phi_\tau^{[k]}$, a defect $\mathbf{w}^{[k]}$ needs to be introduced:

$$\mathbf{u}(t) = \Phi_{t/\varepsilon}^{[k]} \circ \Psi_t^{[k]} \circ (\Phi_0^{[k]})^{-1}(\mathbf{u}(0)) + \mathbf{w}^{[k]}(t), \tag{3.23}$$

to ensure that there are no asymptotical truncations made to the exact solution. The decomposition (3.23) is referred as the MM decomposition of the solution of (3.17).

As a matter of fact, the first order approximation $\Phi_\tau^{[1]}$ given by the MM decomposition, i.e., $k = 0$ in (3.22), coincides with the first order Chapman–Enskog expansion that we introduced in the previous subsection:

$$\Phi_\tau^{[1]}(\mathbf{v}) = \mathbf{v} + \varepsilon A F(\tau, \mathbf{v}) =: \Theta(\tau, \mathbf{v}).$$

Thus, (3.12) or (3.17) has the first order MM decomposition:

$$\mathbf{u}(t) = \Theta(t/\varepsilon, \mathbf{r}(t)) + \mathbf{w}(t), \quad t \geq 0, \tag{3.24}$$

where we denote $\mathbf{r}(t) := \Psi_t^{[1]} \circ (\Phi_0^{[1]})^{-1}(\mathbf{u}(0))$ as the macro part and $\mathbf{w}(t)$ as the micro part. By (3.21), we have

$$F_0^{[1]} = (\Pi D_{\mathbf{v}} \Phi_\tau^{[1]})^{-1} \Pi F(\cdot, \Phi_\tau^{[1]}) = \Pi F(\cdot, \Theta),$$

and then by (3.19), the macro part satisfying the averaged equation reads as

$$\begin{cases} \dot{\mathbf{r}}(t) = \Pi F\left(\cdot, \Theta(\cdot, \mathbf{r}(t))\right), \quad t > 0, \\ \mathbf{r}(0) = \mathbf{u}(0) - \varepsilon A F(\tau, \mathbf{u}(0))|_{\tau=0}. \end{cases} \tag{3.25}$$

Plugging (3.24) into (3.17), we find the equation for the micro part:

$$\begin{cases} \dot{\mathbf{w}}(t) = G(t/\varepsilon, \mathbf{r}(t), \mathbf{w}(t)), \quad t > 0, \\ \mathbf{w}(0) = \varepsilon A \left[F(\tau, \mathbf{u}(0)) - F(\tau, \mathbf{r}(0)) \right] |_{\tau=0}, \end{cases} \tag{3.26}$$

with

$$G(\tau,\mathbf{r},\mathbf{w}) := F\left(\tau,\Theta(\tau,\mathbf{r})+\mathbf{w}\right)-(I-\Pi)F(\tau,\mathbf{r})-\frac{d}{dt}\Theta(\tau,\mathbf{r}(t)).$$

In the first order MM decomposition, the macro part (3.25) is smooth, containing no high frequencies. As for the micro part, it can be shown that [10]

$$\mathbf{w}(t)=O(\varepsilon^2),\quad \partial_t\mathbf{w}(t)=O(\varepsilon),\quad \partial_t^2\mathbf{w}(t)=O(1).$$

Thanks to the reformulation (3.12), we are able to consider this MM approach for the characteristics (3.2).

An integration scheme. Now, based on the MM decomposed systems (3.25) and (3.26), we are going to propose a second order integration for solving (3.17) which is a compact formulation of (3.12) with $\mathbf{u}(t)=\binom{\mathbf{x}(t)}{\mathbf{y}(t)}$ and $F(\tau,\mathbf{u})=\binom{F_{\mathbf{x}}(\tau,\mathbf{x},\mathbf{y})}{F_{\mathbf{y}}(\tau,\mathbf{x},\mathbf{y})}$. We solve the macro part (3.25) by a leap-frog finite difference scheme:

$$\mathbf{r}^{n+1}=\mathbf{r}^{n-1}+2\Delta t\Pi F\left(\cdot,\Theta(\cdot,\mathbf{r}^n)\right),\quad n\geq 1,\quad \mathbf{r}^1=\mathbf{r}^0+\Delta t\Pi F\left(\cdot,\Theta(\cdot,\mathbf{r}^0)\right).$$

For the micro part (3.26), we integrate the equation to have

$$\begin{aligned}\mathbf{w}(t_{n+1})-\mathbf{w}(t_n)&=\int_{t_n}^{t_{n+1}}G(t/\varepsilon,\mathbf{r}(t),\mathbf{w}(t))dt\\ &=\int_{t_n}^{t_{n+1}}H(t/\varepsilon,\mathbf{r}(t),\mathbf{w}(t))dt-\Theta(t_{n+1}/\varepsilon,\mathbf{r}(t_{n+1}))+\Theta(t_n/\varepsilon,\mathbf{r}(t_n)),\end{aligned}\tag{3.27}$$

where

$$H(\tau,\mathbf{r},\mathbf{w}) := F\left(\tau,\Theta(\tau,\mathbf{r})+\mathbf{w}\right).$$

Since $H(\tau,\mathbf{r},\mathbf{w})$ is periodic in $\tau\in\mathbb{T}$, we have a Fourier expansion

$$H(\tau,\mathbf{r},\mathbf{w})=\sum_{l\in\mathbb{Z}}\widehat{H}_l(\mathbf{r},\mathbf{w})\mathrm{e}^{il\tau},$$

and the integration in (3.27) can be approximated as

$$\begin{aligned}&\int_{t_n}^{t_{n+1}}H(t/\varepsilon,\mathbf{r}(t),\mathbf{w}(t))dt=\sum_{l\in\mathbb{Z}}\int_{t_n}^{t_{n+1}}\widehat{H}_l(\mathbf{r}(t),\mathbf{w}(t))\mathrm{e}^{ilt/\varepsilon}dt\\ &\approx\sum_{l\in\mathbb{Z}}\int_{t_n}^{t_{n+1}}\left[\widehat{H}_l(\mathbf{r}(t_n),\mathbf{w}(t_n))+(t-t_n)\frac{d}{dt}\widehat{H}_l(\mathbf{r}(t_n),\mathbf{w}(t_n))\right]\mathrm{e}^{ilt/\varepsilon}dt\\ &\approx\sum_{l\in\mathbb{Z}}\int_{t_n}^{t_{n+1}}\left[\widehat{H}_l(\mathbf{r}(t_n),\mathbf{w}(t_n))+\frac{t-t_n}{\Delta t}\left(\widehat{H}_l(\mathbf{r}(t_n),\mathbf{w}(t_n))-\widehat{H}_l(\mathbf{r}(t_{n-1}),\mathbf{w}(t_{n-1}))\right)\right]\mathrm{e}^{ilt/\varepsilon}dt.\end{aligned}$$

Therefore, for $n\geq 1$,

$$\begin{aligned}\mathbf{w}(t_{n+1})\approx\mathbf{w}(t_n)&+\sum_{l\in\mathbb{Z}}\mathrm{e}^{ilt_n/\varepsilon}\left[\alpha_l\widehat{H}_l(\mathbf{r}(t_n),\mathbf{w}(t_n))+\frac{\beta_l}{\Delta t}\left(\widehat{H}_l(\mathbf{r}(t_n),\mathbf{w}(t_n))-\widehat{H}_l(\mathbf{r}(t_{n-1}),\mathbf{w}(t_{n-1}))\right)\right]\\ &-\Theta(t_{n+1}/\varepsilon,\mathbf{r}(t_{n+1}))+\Theta(t_n/\varepsilon,\mathbf{r}(t_n)),\end{aligned}$$

and as for $n=0$,

$$\mathbf{w}(t_1)\approx\mathbf{w}(0)+\sum_{l\in\mathbb{Z}}\alpha_l\widehat{H}_l(\mathbf{r}(0),\mathbf{w}(0))-\Theta(t_1/\varepsilon,\mathbf{r}(t_1))+\Theta(0,\mathbf{r}(0)),$$

where

$$\alpha_l = \int_0^{\Delta t} \mathrm{e}^{ilt/\varepsilon} dt = \begin{cases} \dfrac{i\varepsilon}{l}\left(1 - \mathrm{e}^{\frac{il\Delta t}{\varepsilon}}\right), & l \neq 0, \\ \Delta t, & l = 0, \end{cases}$$

$$\beta_l = \int_0^{\Delta t} t\mathrm{e}^{ilt/\varepsilon} dt = \begin{cases} \dfrac{\varepsilon}{l^2}\left((\varepsilon - il\Delta t)\mathrm{e}^{\frac{il\Delta t}{\varepsilon}} - \varepsilon\right), & l \neq 0, \\ \dfrac{\Delta t^2}{2}, & l = 0. \end{cases}$$

In total, the detailed exponential integration scheme based on the MM method reads as

$$\mathbf{u}^{n+1} = \Theta(t_{n+1}/\varepsilon, \mathbf{r}^{n+1}) + \mathbf{w}^{n+1}, \quad n \geq 0, \tag{3.28a}$$

$$\mathbf{r}^{n+1} = \mathbf{r}^{n-1} + 2\Delta t \Pi F\left(\cdot, \Theta(\cdot, \mathbf{r}^n)\right), \quad n \geq 1, \tag{3.28b}$$

$$\begin{aligned} \mathbf{w}^{n+1} = \mathbf{w}^n + \sum_{l=-N_\tau/2}^{N_\tau/2-1} \mathrm{e}^{ilt_n/\varepsilon}\left[\alpha_l \widehat{H}_l(\mathbf{r}^n, \mathbf{w}^n) + \frac{\beta_l}{\Delta t}\left(\widehat{H}_l(\mathbf{r}^n, \mathbf{w}^n) - \widehat{H}_l(\mathbf{r}^{n-1}, \mathbf{w}^{n-1})\right)\right] \\ - \Theta(t_{n+1}/\varepsilon, \mathbf{r}^{n+1}) + \Theta(t_n/\varepsilon, \mathbf{r}^n), \quad n \geq 1, \end{aligned} \tag{3.28c}$$

$$\mathbf{r}^1 = \mathbf{r}^0 + \Delta t \Pi F\left(\cdot, \Theta(\cdot, \mathbf{r}^0)\right), \quad \mathbf{w}^1 = \mathbf{w}^0 + \sum_{l=-N_\tau/2}^{N_\tau/2-1} \alpha_l \widehat{H}_l(\mathbf{r}^0, \mathbf{w}^n) - \Theta(t_1/\varepsilon, \mathbf{r}^1) + \Theta(0, \mathbf{r}^0), \tag{3.28d}$$

$$\mathbf{r}^0 = \mathbf{u}(0) - \varepsilon A F(\tau, \mathbf{u}(0))|_{\tau=0}, \quad \mathbf{w}^0 = \varepsilon A\left[F(\tau, \mathbf{u}(0)) - F(\tau, \mathbf{r}(0))\right]|_{\tau=0}, \tag{3.28e}$$

where N_τ is an even integer to truncate the Fourier series. Suppose the numerical solution of MM is obtained as $\mathbf{u}^n = \binom{\mathbf{x}^n}{\mathbf{y}^n}$; then the numerical velocity of (3.2) at t_n is given as

$$\mathbf{v}^n = \cos(t_n/\varepsilon)\mathbf{y}^n + (1 - \cos(t_n/\varepsilon))(\mathbf{B}(\mathbf{x}^n) \cdot \mathbf{y}^n)\mathbf{B}(\mathbf{x}^n) + \sin(t_n/\varepsilon)\mathbf{y}^n \times \mathbf{B}(\mathbf{x}^n).$$

The MM scheme (3.28) is uniformly second order accurate. In practical programming, one only needs a subroutine to evaluate $F(\tau, \mathbf{u})$. When the electric and magnetic field $\mathbf{E}$ and $\mathbf{B}$ in particle system (3.2) are given external functions such as polynomials, the dependence of the fast time scale t/ε (or τ) in F and Θ can be found out explicitly and the averaging with respect to τ (through the operator Π) in the MM scheme can be pre-computed exactly. Then the MM method will have a discretization error in time of $O(\Delta t^2)$ with optimal computational cost $O(\Delta t^{-1})$. In case that the exact evaluation of t/ε is impossible or too costly, one can always perform those computations of the fast time scale with the additional variable τ by FFT with uniform spectral accuracy thanks to the periodicity. In such a case, the error bound of MM is

$$O(\Delta t^2 + N_\tau^{-m_0}),$$

with $m_0 > 0$ arbitrarily large (due to smoothness in τ and periodicity) and the total cost being $O(\Delta t^{-1} N_\tau \log N_\tau)$, which are the same for TSF.

Full recovery of oscillation. Since MM method finds out the dependence of the fast scale in a rather explicit way, it can easily recover the complete gyro-motion of the particles, i.e., the full oscillatory trajectory of the solution of (3.2), by interpolating the macro part and micro part, respectively.

Let $\mathbf{r}^n$ and $\mathbf{w}^n$ be the numerical solutions obtained from MM under a step size $\Delta t > 0$. For an arbitrary $t > 0$, if $t_n < t < t_{n+1}$, then we can use the linear interpolation to get

$$\mathbf{r}_I^n(t) = \frac{t_{n+1} - t}{\Delta t}\mathbf{r}^n + \frac{t - t_n}{\Delta t}\mathbf{r}^{n+1}, \quad \mathbf{w}_I^n(t) = \frac{t_{n+1} - t}{\Delta t}\mathbf{w}^n + \frac{t - t_n}{\Delta t}\mathbf{w}^{n+1}.$$

Noting that $\mathbf{r}(t)$ is the averaged part and $\mathbf{w}(t)$ satisfies $\partial_t^2 \mathbf{w}(t) = O(1)$, together with the accuracy order of $\mathbf{r}^n$ and $\mathbf{w}^n$ from the MM scheme, it is clear that the above linear interpolation gives uniform second accuracy for approximating $\mathbf{r}(t)$ and $\mathbf{w}(t)$. Then, with MM decomposition (3.24), we get the interpolated numerical solution of (3.17),

$$\mathbf{u}_I^n(t) = \Theta(t/\varepsilon, \mathbf{r}_I^n(t)) + \mathbf{w}_I^n(t), \quad t_n \le t \le t_{n+1}, \tag{3.29}$$

which fully recovers the oscillation information with ease. It is direct to see that

$$|\mathbf{u}(t) - \mathbf{u}_I^n(t)| = O(\Delta t^2 + N_\tau^{-m_0}).$$

Restart strategy. In practical long time computing, we observe that the MM scheme (3.28) could have numerical instability issues. The instability is developed from the micro part (3.26) in MM decomposition (3.24) as time evolves since $\mathbf{w}(t) = O(\varepsilon)$ does not hold for arbitrary long times in general. Here we propose a restart strategy to improve its long time performance.

Choose $T_0 > 0$ as the period to restart the MM decomposition. For some $m \in \mathbb{N}$, we consider the oscillatory problem (3.17) for $\mathbf{u}^m(t) = \mathbf{u}(mT_0 + t)$ as

$$\dot{\mathbf{u}}^m(t) = F(mT_0/\varepsilon + t/\varepsilon, \mathbf{u}^m(t)), \quad 0 < t \le T_0.$$

Then we apply the proposed MM strategy to the above, which leads to MM decomposition as

$$\mathbf{u}^m(t) = \Theta(mT_0/\varepsilon + t/\varepsilon, \mathbf{r}(t)) + \mathbf{w}(t), \quad 0 \le t \le T_0, \tag{3.30}$$

with

$$\begin{cases} \dot{\mathbf{r}}(t) = \Pi F\left(mT_0/\varepsilon + \cdot, \Theta(mT_0/\varepsilon + \cdot, \mathbf{r}(t))\right), \quad 0 < t \le T_0, \\ \mathbf{r}(0) = \mathbf{u}^m(0) - \varepsilon A F(mT_0/\varepsilon + \tau, \mathbf{u}^m(0))|_{\tau=0} \end{cases}$$

and

$$\begin{cases} \dot{\mathbf{w}}(t) = G(mT_0/\varepsilon + t/\varepsilon, \mathbf{r}(t), \mathbf{w}(t)), \quad 0 < t \le T_0, \\ \mathbf{w}(0) = \varepsilon A\left[F(mT_0/\varepsilon + \tau, \mathbf{u}^m(0)) - F(mT_0/\varepsilon + \tau, \mathbf{r}(0))\right]|_{\tau=0}. \end{cases}$$

The integration scheme (3.28) is then applied to solve the above two systems.

As can be seen in the numerical results later, this restart strategy for solving (3.2) is stable in long time computing. Its accuracy and computational cost are essentially the same as the direct scheme without restart.

Remark 3.1. In the case that $\mathbf{B}(\mathbf{x}) = \mathbf{B}_0(\mathbf{x}) + O(\varepsilon)$, with $|\mathbf{B}_0(\mathbf{x})| \equiv$ const, all the proposed algorithms in this section can be extended to such a case without any essential difficulties.

Remark 3.2. Although physically the magnetic field should be divergence-free, i.e., $\nabla_{\mathbf{x}} \cdot \mathbf{B} = 0$, all the algorithms we proposed in this section do not rely on the divergence-free property of $\mathbf{B}(\mathbf{x})$ to offer the uniform accuracy.

4. Extension to varying intensity magnetic field. In this section, we extend previous methods to the case of a Vlasov equation with a general magnetic field (whose intensity may vary), i.e.,

$$|\mathbf{B}(\mathbf{x})| = b(\mathbf{x}) \neq \text{const}, \quad \mathbf{x} \in \mathbb{R}^3.$$

We start by commenting on the difficulties to be encountered in this situation. As soon as $|\mathbf{B}(\mathbf{x})| = b(\mathbf{x})$ varies with $\mathbf{x}$ while remaining bounded from below by some c_0 independent of ε, the characteristic equations for each particle

$$\begin{aligned}\dot{\mathbf{x}}_k(t) &= \mathbf{v}_k(t),\\ \dot{\mathbf{v}}_k(t) &= \mathbf{E}(t,\mathbf{x}_k(t)) + \frac{1}{\varepsilon}\mathbf{v}_k(t)\times\mathbf{B}(\mathbf{x}_k(t)), \quad t>0,\end{aligned}$$

generate high oscillations. However, the dynamics of the dominant part of the whole particle system is nonperiodic in general and thus does not allow for the application of averaging techniques. A possible remedy consists in time-reparametrization. However, another difficulty then arises from the Poisson equation itself:

$$\nabla_{\mathbf{x}}\cdot\mathbf{E}(t,\mathbf{x}) = \sum_{k=1}^{N_p} w_k\delta(\mathbf{x}-\mathbf{x}_k(t)),$$

which couples a huge number ($N_p \gg 1$) of particles with different frequencies.

Rescaling the time for each particle. Each particle has a periodic oscillation with respect to its own time $s_k = s_k(t)$, given by

$$\dot{s}_k(t) = b(\mathbf{x}_k(t)), \quad s_k(0) = 0. \tag{4.1}$$

Note that $s_k(t)$ is strictly increasing and that

$$s_k(t)\to\infty, \quad \text{as} \quad t\to\infty,$$

since $b(\mathbf{x}) \geq c_0 > 0$. Denoting $\tilde{\mathbf{x}}_k(s_k) := \mathbf{x}_k(t)$, $\tilde{\mathbf{v}}_k(s_k) := \mathbf{v}_k(t)$, we indeed have

$$\begin{cases}\dfrac{\mathrm{d}}{\mathrm{d}s_k}\tilde{\mathbf{x}}_k(s_k) = \dfrac{\tilde{\mathbf{v}}_k(s_k)}{b(\tilde{\mathbf{x}}_k(s_k))},\\ \dfrac{\mathrm{d}}{\mathrm{d}s_k}\tilde{\mathbf{v}}_k(s_k) = \dfrac{\mathbf{E}(t(s_k),\tilde{\mathbf{x}}_k(s_k))}{b(\tilde{\mathbf{x}}_k(s_k))} + \dfrac{1}{\varepsilon}\tilde{\mathbf{v}}_k(s_k)\times\dfrac{\mathbf{B}(\tilde{\mathbf{x}}_k(s_k))}{b(\tilde{\mathbf{x}}_k(s_k))}, \quad s_k>0,\\ \tilde{\mathbf{x}}_k(0) = \mathbf{x}_{k,0}, \quad \tilde{\mathbf{v}}_k(0) = \mathbf{v}_{k,0},\end{cases} \tag{4.2}$$

where the intensity of the magnetic field is scaled to one. Assuming that the electric field $\mathbf{E}(t,\mathbf{x})$ is a given external field with no ε-dependent oscillation in t, then the particle system (4.2) is decoupled for each k. Therefore, the numerical methods introduced in the previous section can all be applied to (4.2) for each particle in its own time s_k with uniform accuracy.

In order to build up an approximation of the function $f^\varepsilon(t,\mathbf{x},\mathbf{v})$ through (3.1), it is then necessary to resynchronize for all particles. However, reverting s_k to the physical time t is not straightforward, as it requires numerically solving the nonlinear equation (4.1) or its equivalent for the inverse map:

$$\dot{t}(s_k) = 1/b(\tilde{\mathbf{x}}_k(s_k)), \quad t(0) = 0. \tag{4.3}$$

Given a physical time $t = T > 0$ (or, conversely, $S_k > 0$), the best we can hope for is to determine $s_k(T)$ (or, conversely, $t(S_k)$) up to an error of size $O(\Delta t^p)$ if a pth order numerical method is applied. This source of possible error needs to be properly controlled. Here we illustrate how it can be done for the MM method.

Interpolating to synchronize. For the sake of brevity, we omit k and denote

$$\tilde{\mathbf{B}}(\tilde{\mathbf{x}}) = \frac{\mathbf{B}(\tilde{\mathbf{x}})}{b(\tilde{\mathbf{x}})}, \quad \tilde{\mathbf{E}}(t,\tilde{\mathbf{x}}) = \frac{\mathbf{E}(t,\tilde{\mathbf{x}})}{b(\tilde{\mathbf{x}})}.$$

We filter (4.2) and (4.3) as before by introducing

(4.4)
$$\tilde{\mathbf{y}}(s) := \cos(s/\varepsilon)\tilde{\mathbf{v}}(s) + (1-\cos(s/\varepsilon))(\tilde{\mathbf{B}}(\tilde{\mathbf{x}}(s))\cdot\tilde{\mathbf{v}}(s))\tilde{\mathbf{B}}(\tilde{\mathbf{x}}(s)) - \sin(s/\varepsilon)\tilde{\mathbf{v}}(s)\times\tilde{\mathbf{B}}(\tilde{\mathbf{x}}(s)),$$

and obtain

(4.5)
$$\begin{cases} \dfrac{\mathrm{d}}{\mathrm{d}s}\tilde{\mathbf{x}}(s) = \tilde{F}_{\mathbf{x}}(s/\varepsilon,\tilde{\mathbf{x}}(s),\tilde{\mathbf{y}}(s)), \\ \dfrac{\mathrm{d}}{\mathrm{d}s}\tilde{\mathbf{y}}(s) = \tilde{F}_{\mathbf{y}}(s/\varepsilon,\tilde{\mathbf{x}}(s),\tilde{\mathbf{y}}(s)), \quad s>0, \\ \dfrac{\mathrm{d}}{\mathrm{d}s}t(s) = \dfrac{1}{b(\tilde{\mathbf{x}}(s))}, \\ \tilde{\mathbf{x}}(0) = \mathbf{x}_0, \quad \tilde{\mathbf{y}}(0) = \mathbf{v}_0, \quad t(0) = 0, \end{cases}$$

which now has the appropriate format (3.17). Here $\tilde{F}_{\mathbf{y}}$ is defined similarly as in (3.12) (see section 3.2) with the scaled vector fields $\tilde{\mathbf{E}}$, $\tilde{\mathbf{B}}$, and $\tilde{F}_{\mathbf{x}} = F_{\mathbf{x}}/b(\tilde{\mathbf{x}})$. We then solve system (4.5) with the MM scheme (3.28) with time step $\Delta s > 0$ and denote $t^n \approx t(s_n)$ the numerical solution of $t(s_n)$ at $s_n = n\Delta s$. Then, using the notations $\mathbf{r} := (\mathbf{r}_{\mathbf{x}}, \mathbf{r}_{\mathbf{y}})$ and $\mathbf{w} = (\mathbf{w}_{\mathbf{x}}, \mathbf{w}_{\mathbf{y}})$ for the macro and micro parts (see section 3.3), the numerical solution of $\tilde{\mathbf{x}}$ and $\tilde{\mathbf{y}}$ at $s_n = n\Delta s$ is

$$\tilde{\mathbf{x}}^n := \mathbf{r}_{\mathbf{x}}^n + \varepsilon A\tilde{F}_{\mathbf{x}}(s_n/\varepsilon,\mathbf{r}_{\mathbf{x}}^n,\mathbf{r}_{\mathbf{y}}^n) + \mathbf{w}_{\mathbf{x}}^n \approx \tilde{\mathbf{x}}(s_n), \quad \tilde{\mathbf{y}}^n := \mathbf{r}_{\mathbf{y}}^n + \varepsilon A\tilde{F}_{\mathbf{y}}(s_n/\varepsilon,\mathbf{r}_{\mathbf{x}}^n,\mathbf{r}_{\mathbf{y}}^n) + \mathbf{w}_{\mathbf{y}}^n \approx \tilde{\mathbf{y}}(s_n).$$

Assume that $b(\cdot) \in C^1(\mathbb{R}^3)$ and $0 < c_0 \le b(\mathbf{x}) \le C_b$ for all $\mathbf{x} \in \mathbb{R}^3$ for some $C_b > 0$. Then from

$$t^n \ge t(s_n) - |t^n - t(s_n)| \ge \frac{s_n}{C_b} - C\Delta s^2$$

we see that whenever $\Delta s > 0$ is small enough, the value of t^n will eventually become greater than any arbitrary positive value. For a given final time $T > 0$, we thus stop the algorithm when $t^n \le T \le t^{n+1}$. Note that the function $t(s)$ satisfies

$$\frac{\mathrm{d}^2}{\mathrm{d}s^2}t(s) = O(1), \quad 0 < \varepsilon \le 1,$$

so that we can interpolate the value of $t(s)$ from t^n and t^{n+1} with second order uniform accuracy:

$$\theta := \frac{T - t^{n+1}}{t^n - t^{n+1}}, \quad T = \theta t^n + (1-\theta)t^{n+1}, \quad s^* = \theta s^n + (1-\theta)s^{n+1}.$$

Interpolation is further used to obtain

$$\mathbf{r}_{\mathbf{x}}^* = \theta\mathbf{r}_{\mathbf{x}}^n + (1-\theta)\mathbf{r}_{\mathbf{x}}^{n+1}, \quad \mathbf{r}_{\mathbf{y}}^* = \theta\mathbf{r}_{\mathbf{y}}^n + (1-\theta)\mathbf{r}_{\mathbf{y}}^{n+1},$$
$$\mathbf{w}_{\mathbf{x}}^* = \theta\mathbf{w}_{\mathbf{x}}^n + (1-\theta)\mathbf{w}_{\mathbf{x}}^{n+1}, \quad \mathbf{w}_{\mathbf{y}}^* = \theta\mathbf{w}_{\mathbf{y}}^n + (1-\theta)\mathbf{w}_{\mathbf{y}}^{n+1}.$$

As stated in section 3.3, all functions used above in the interpolation have a uniformly bounded second order derivative. As a consequence, the so-obtained approximations

are uniformly second order. Eventually, the numerical solutions of (4.5) at $s = s(T)$ are given by

$$\tilde{\mathbf{x}}(s(T)) \approx \tilde{\mathbf{x}}^*, \quad \tilde{\mathbf{y}}(s(T)) \approx \tilde{\mathbf{y}}^*,$$

with

$$\tilde{\mathbf{x}}^* := \mathbf{r}_{\mathbf{x}}^* + \varepsilon A\tilde{F}_{\mathbf{x}}(s^*/\varepsilon, \mathbf{r}_{\mathbf{x}}^*, \mathbf{r}_{\mathbf{y}}^*) + \mathbf{w}_{\mathbf{x}}^*, \quad \tilde{\mathbf{y}}^* := \mathbf{r}_{\mathbf{y}}^* + \varepsilon A\tilde{F}_{\mathbf{y}}(s^*/\varepsilon, \mathbf{r}_{\mathbf{x}}^*, \mathbf{r}_{\mathbf{y}}^*) + \mathbf{w}_{\mathbf{y}}^*. \tag{4.6}$$

Note that the dependence in the fast-time s/ε within the MM method only appears in the $O(\varepsilon)$-terms. As a consequence, the approximation errors of $\tilde{\mathbf{x}}(s(T))$ and $\tilde{\mathbf{y}}(s(T))$ by (4.6) are still of uniform second order, although an error is introduced on s^*/ε owing to $|s(T) - s^*|/\varepsilon = O(\Delta s^2/\varepsilon)$.

To reconstruct an approximation of the distribution function $f^\varepsilon(T, \mathbf{x}, \mathbf{v})$, we need $\mathbf{x}(T)$ and $\mathbf{v}(T)$. For the position variable, we directly have $\mathbf{x}(T) = \tilde{\mathbf{x}}(s(T))$ due to the definition. As for the velocity variable $\mathbf{v}(T)$, we need to invert the change of variables (4.4), where the fast-scale s/ε occurs in some $O(1)$-terms. However, the parallel component $\mathbf{v}_\parallel := (\mathbf{B} \cdot \mathbf{v})\mathbf{B}/\|\mathbf{B}\|^2$ of the velocity as well as $|\mathbf{v}|$ do not suffer from the same problem, thanks to the following observations (let us recall that $\|\tilde{\mathbf{B}}(\tilde{\mathbf{x}}(s))\|^2 = 1$):

$$\tilde{\mathbf{v}}_\parallel(s) = (\tilde{\mathbf{B}}(\tilde{\mathbf{x}}(s)) \cdot \tilde{\mathbf{y}}(s))\tilde{\mathbf{B}}(\tilde{\mathbf{x}}(s)), \quad |\tilde{\mathbf{v}}(s)| = |\tilde{\mathbf{y}}(s)|,$$

which allow us to get

$$\mathbf{v}_\parallel(T) \approx (\tilde{\mathbf{B}}(\tilde{\mathbf{x}}(s(T))) \cdot \tilde{\mathbf{y}}(s(T)))\tilde{\mathbf{B}}(\tilde{\mathbf{x}}(s(T))), \quad |\mathbf{v}(T)| = |\tilde{\mathbf{y}}(s(T))|.$$

Therefore, the strategy proposed in this section is of overall uniform second order for the computation of

$$\mathbf{x}(t), \quad \mathbf{v}_\parallel(t), \quad |\mathbf{v}(t)|, \qquad t \geq 0.$$

This, in turn, allows for a uniformly accurate approximation of macroscopic quantities such as the density or the kinetic energy

$$\rho^\varepsilon(t, \mathbf{x}) := \int_{\mathbb{R}^3} f^\varepsilon(t, \mathbf{x}, \mathbf{v}) d\mathbf{v}, \quad \rho_{\mathbf{v}}^\varepsilon(t, \mathbf{x}) := \int_{\mathbb{R}^3} |\mathbf{v}|^2 f^\varepsilon(t, \mathbf{x}, \mathbf{v}) d\mathbf{v},$$

as well as the magnetic moment [26, 32]

$$\mu^\varepsilon(t) := \int_{\mathbb{R}^3} \int_{\mathbb{R}^3} f^\varepsilon(t, \mathbf{x}, \mathbf{v}) \frac{|\mathbf{v}_\perp|^2}{|\mathbf{B}(\mathbf{x})|} d\mathbf{x} d\mathbf{v}, \tag{4.7}$$

with $\mathbf{v}_\perp := \mathbf{v} - \mathbf{v}_\parallel$.

5. Numerical results. This section is devoted to presenting the numerical results from the proposed numerical schemes. We shall first test and compare the accuracy, efficiency, and long time performance of the schemes considering a single test particle for some three dimensional simulations in the two following cases: a constant intensity magnetic field and a varying intensity magnetic field. Then we shall focus on the nonlinear Vlasov–Poisson case under the influence of a constant intensity magnetic field.

5.1. Accuracy study. We investigate the performance of the proposed numerical methods by considering a single particle system in three dimensions:

$$\begin{aligned} &\dot{\mathbf{x}}(t) = \mathbf{v}(t), \\ &\dot{\mathbf{v}}(t) = \mathbf{E}(\mathbf{x}(t)) + \frac{1}{\varepsilon}\mathbf{v}(t) \times \mathbf{B}(\mathbf{x}(t)), \quad t > 0, \\ &\mathbf{x}(0) = \mathbf{x}_0, \quad \mathbf{v}(0) = \mathbf{v}_0. \end{aligned} \tag{5.1}$$

We take two three dimensional vector fields $\mathbf{B}(\mathbf{x}) : \mathbf{x} \in \mathbb{R}^3 \to \mathbb{R}^3$ and $\mathbf{E}(\mathbf{x}) = -\nabla_{\mathbf{x}}\phi(\mathbf{x})$, with some $\phi(\mathbf{x}) : \mathbb{R}^3 \to \mathbb{R}$; then (5.1) is a Hamiltonian system with the energy conserved as

$$\mathcal{H}_s(t) := \frac{1}{2}|\mathbf{v}(t)|^2 + \phi(\mathbf{x}(t)) = \mathcal{H}_s(0), \qquad t \geq 0. \tag{5.2}$$

Note here that we do not require $\mathbf{B}$ to be divergence-free for these accuracy tests since all the presented properties of the proposed schemes hold in general as long as $\mathbf{B}$ is a smooth enough vector field. Hence, we first focus on a constant intensity magnetic field before considering the general case to test the proposed methods MRC, TSF, and MM.

Example 5.1 (constant intensity). We take the two external fields in the system (5.1):

$$\mathbf{E}(\mathbf{x}) = \begin{pmatrix} \cos(x_1/2)\sin(x_2)\sin(x_3)/2 \\ \sin(x_1/2)\cos(x_2)\sin(x_3) \\ \sin(x_1/2)\sin(x_2)\cos(x_3) \end{pmatrix},$$
$$\mathbf{B}(\mathbf{x}) = \begin{pmatrix} \sin(x_1+x_2) \\ \cos(x_1+x_2)\sin(x_3) \\ \cos(x_1+x_2)\cos(x_3) \end{pmatrix}, \quad \mathbf{x} = (x_1, x_2, x_3),$$

where $|\mathbf{B}(\mathbf{x})| = 1$ and $\mathbf{E}(\mathbf{x})$ derives from the potential $\phi(\mathbf{x})$:

$$\mathbf{E}(\mathbf{x}) = -\nabla_{\mathbf{x}}\phi(\mathbf{x}), \quad \phi(\mathbf{x}) = -\sin(x_1/2)\sin(x_2)\sin(x_3).$$

We choose the initial data for (5.1) as

$$\mathbf{x}_0 = (1/3, -1/2, \sqrt{\pi}/2), \quad \mathbf{v}_0 = (1/2, \mathrm{e}/4, -1/3).$$

A reference solution is obtained by using the classical fourth order Runge–Kutta (RK4) method with small step size $\Delta t = 10^{-6}$.

We first study the convergence of the three proposed methods (MRC, TSF, and MM) aiming to illustrate their uniform accuracy for all $\varepsilon \in]0, 1]$. To do so, we solve the system under different ε until $T = \pi/2$ and compute the error

$$error = \frac{|\mathbf{x}(T) - \mathbf{x}^{num}|}{|\mathbf{x}(T)|} + \frac{|\mathbf{v}(T) - \mathbf{v}^{num}|}{|\mathbf{v}(T)|}, \tag{5.3}$$

where $\mathbf{x}^{num}$ and $\mathbf{v}^{num}$ are the numerical values obtained by the different schemes. For the TSF and MM methods, we define the time step $\Delta t = T/M$, with $M \in \mathbb{N}^\star$, and we fix the grid points for the τ-direction as $N_\tau = 32$. For MRC, we define the

numerical parameters from a given $M \in \mathbb{N}^\star$ as follows: $H = \varepsilon M_f/M$ and $h = 2\pi/M$ if $M_f/M \geq 1$ and $\Delta t = 2\pi/M$ if $M_f/M < 1$ (M_f being defined by (3.4)).

The error (defined by (5.3)) produced by the three methods at $T = \pi/2$ with respect to the number of (macro) grid points M or with respect to ε is given in Figure 1. As expected, the three methods enjoy the uniform second order accuracy property since the rate of convergence is essentially insensitive to the value $\varepsilon \in]0, 1]$. The typical behavior of uniformly accurate methods can be observed on the error as a function of ε: the curves obtained for different M are almost parallel. Note that the results obtained by TSF and MM are very close, whereas the error produced by MRC becomes smaller when ε decreases.

In Figure 2, we look at the error of TSF and MM with respect to the number of grid points N_τ in the auxiliary variable τ (the time step is fixed to $\Delta t = 10^{-5}$). This error is important to study since these two methods involve an additional variable τ which may make them less competitive. We can see in Figure 2 that the error decreases spectrally as the number of grid points N_τ increases. Moreover, for small values of ε, a very small number of N_τ is needed to reach high accuracy: $\varepsilon \leq 2^{-7}$, $N_\tau = 16$ is enough for machine precision. Finally, let us remark that the results obtained for MM are much less sensitive than TSF: when $\varepsilon = 1/2$, $N_\tau = 32$ enables us to reach machine precision for MM, whereas TSF requires $N_\tau = 128$.

We now intend to compare the efficiency of TSF, MM, and MRC in different regimes ($\varepsilon = 1/2$ and $1/2^{14}$). Let us first fix the numerical parameters. According to the previous comments, in the regime $\varepsilon = 1/2$ we take $N_\tau = 128$ for TSF and $N_\tau = 32$ for MM, whereas in the regime $\varepsilon = 1/2^{14}$ we take $N_\tau = 8$ for both TSF and MM. We test the long time behavior of the three methods by investigating the relative error on the numerical total energy defined by

$$error(t^n) = \frac{|\mathcal{H}_s^n - \mathcal{H}_s(0)|}{|\mathcal{H}_s(0)|}, \quad \mathcal{H}_s^n = \frac{1}{2}|\mathbf{v}^n|^2 + \phi(\mathbf{x}^n), \tag{5.4}$$

where $\mathcal{H}_s^n$ is the numerical approximation of $\mathcal{H}_s(t_n)$ given by (5.2). We plot in Figure 3 the error (considering the maximum of (5.4) among all the iterations) against the computational time of the three methods for $\varepsilon = 1/2$ or $1/2^{14}$ (different time steps have been chosen). For a given error, when $\varepsilon = 1/2$ the MRC method is more efficient than TSF or MM, but it is no longer true when ε becomes smaller. This is explained by the fact that N_τ can be chosen smaller in the asymptotic regime, making TSF and MM more competitive. MRC for $\varepsilon = 1/2$ reads as the Strang splitting, while for $\varepsilon = 1/2^{14}$ the convergence of MRC becomes first order in terms of total computational cost. For a comparison with the classical method, we also include the efficiency curve of RK4 in the limit regime in Figure 3. Then, in Figure 4, the time history of (5.4) is plotted for the three methods until $T = 32\pi$ for $\varepsilon = 1/2^{14}$. The TSF and MM methods run with $N_\tau = 32$ and $M = 1024$ ($\Delta t = 0.098$) or $M = 2048$ ($\Delta t = 0.049$). We report that, for this test, MM becomes unstable in large time so that the restart strategy is used every $T_0 = 8\pi$. For MRC, we used $M = 64$ or $M = 128$. Figure 4 clearly shows that MRC has the best long time behavior among the three methods. Indeed, TSF and MM have a linear drift in the energy error as time evolves, whereas for MRC it remains of the same order (about 10^{-5}) for large time. Let us remark that the energy error converges quadratically for the three methods with respect to number of time grid points M.

Finally, we consider the scheme MM ($M = 32$, $N_\tau = 32$) to illustrate the reconstruction of the whole trajectory for $t \in [0, \pi]$ (so that $\Delta t = 0.0982$). To do so, we still consider the system (5.1) with Example 5.1, with $\varepsilon = 1/2^5$. In Figure 5, we plot a

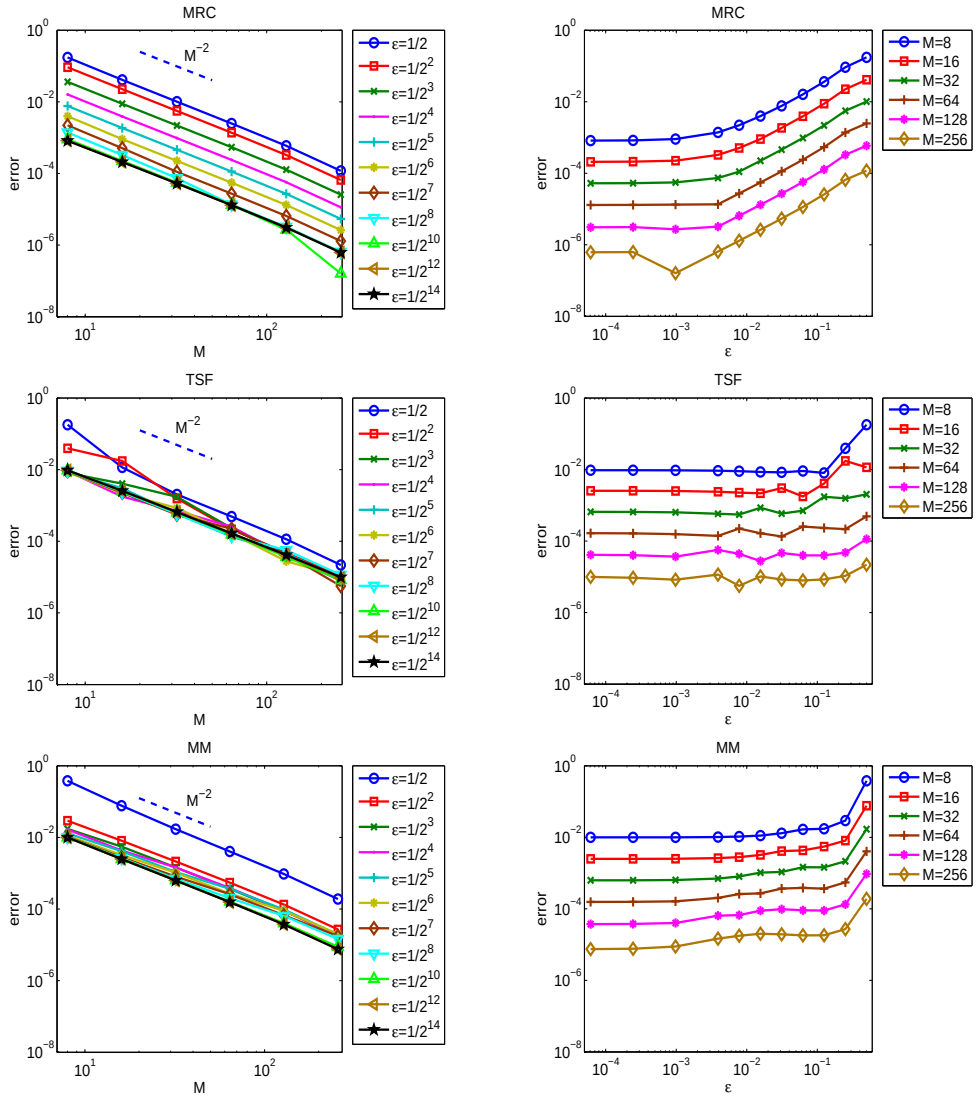

FIG. 1. *Errors of MRC, TSF, and MM with respect to time steps M under different ε (left) or with respect to ε under different M (right) for Example* 5.1.

reference trajectory (obtained with a very small time step) and the numerical solution obtained by MM using the strategy proposed in section 3.3 (i.e., with a coarse time grid and using the linear interpolation strategy in (3.29)). Using a few grid points, we can see that the MM method is able to fully restore the complex trajectory (highly oscillatory confined behavior around a magnetic field line) of the particle under trivial computational cost.

Example 5.2 (varying intensity). Second, we investigate the numerical performance of the strategy proposed in section 4 for a magnetic field with varying direction and varying intensity on the particle system (5.1).

We shall consider the particle system (5.1) with the same electric field $\mathbf{E}(\mathbf{x})$ as

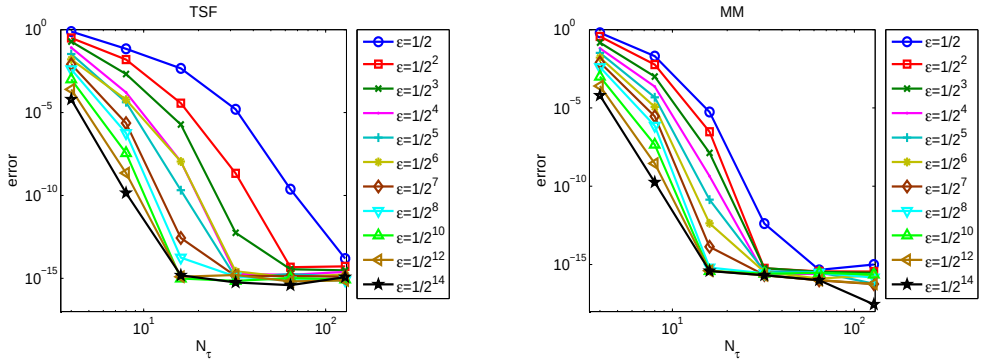

FIG. 2. *Error of TSF and MM with respect to N_τ under different ε for Example* 5.1.

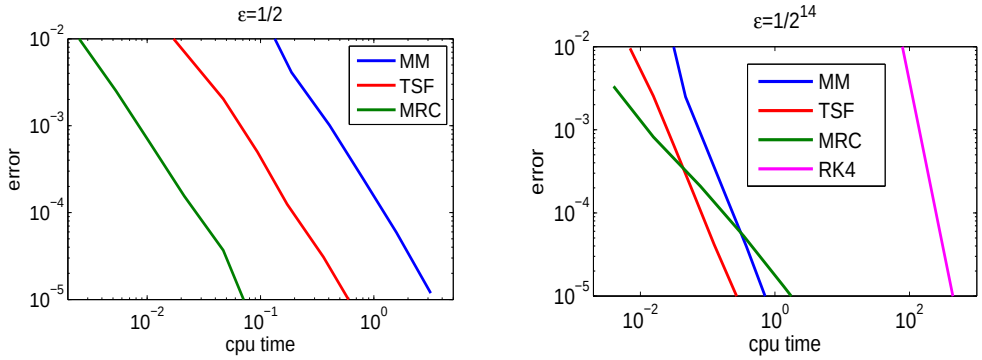

FIG. 3. *Efficiency comparison of TSF, MM, and MRC in the classical (left) or asymptotic regime (right) of ε for Example* 5.1: *error versus computational time.*

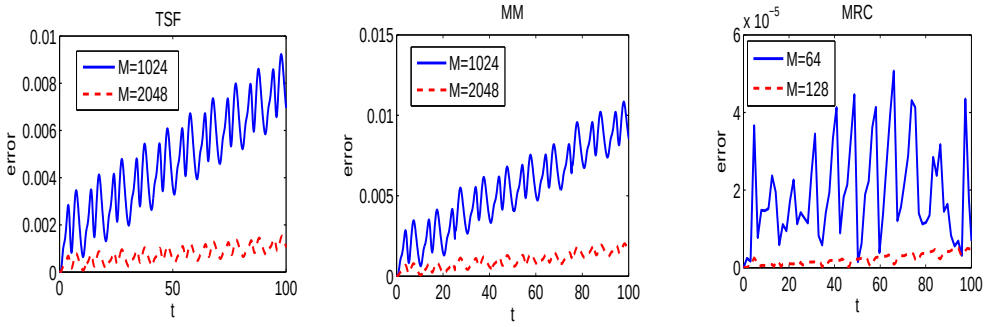

FIG. 4. *Energy error of TSF, MM (with restart every $T_0 = 8\pi$), and MRC for Example* 5.1 *under $\varepsilon = 1/2^{14}$ until $T = 32\pi$. $\Delta t = 0.0982$ or 0.0491 (ratio $\Delta t/\varepsilon \approx 1609$ or 804) for TSF and MM.*

before, but here the magnetic field is

$$\mathbf{B}(\mathbf{x}) = \begin{pmatrix} 1 - \sin(x_2)/2 \\ 1 + \cos(x_3)/2 \\ 1 + \cos(x_1)/2 \end{pmatrix}, \quad \mathbf{x} = (x_1, x_2, x_3),$$

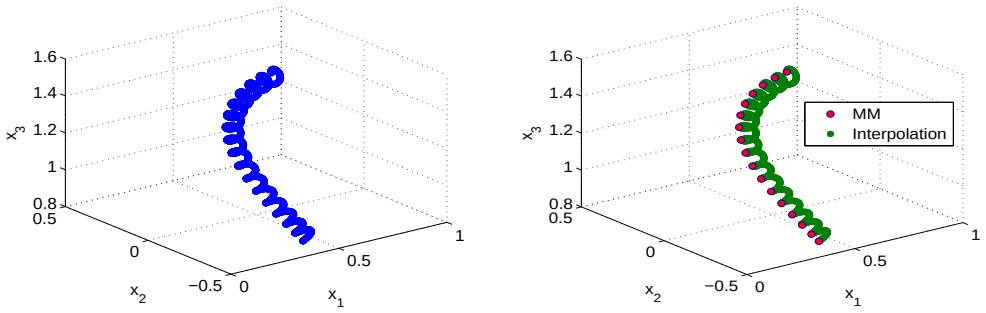

FIG. 5. *Left: exact trajectory of the particle in Example* 5.1 *until* $T = \pi$ *under* $\varepsilon = 1/2^5$. *Right: numerical solution of MM under* $\Delta t = 0.0982$ *(red dots, ratio* $\Delta t/\varepsilon \approx 3.14$*) and the fully recovered trajectory with fine linear interpolation. Color is available online only.*

which satisfies $\nabla_{\mathbf{x}} \cdot \mathbf{B} = 0$ but has a varying intensity in $\mathbf{x} \in \mathbb{R}^3$ since

$$|\mathbf{B}(\mathbf{x})|^2 = 3 + \cos(x_1) + \cos(x_3) - \sin(x_2) + \cos(x_1)^2/4 + \sin(x_2)^2/4 + \cos(x_3)^2/4.$$

We choose the same initial data as before for Example 5.1 and solve the problem via the new time formulation (4.2) with the MM method (see section 4). The reference solution is again obtained by directly solving (5.1) with the RK4 method under small step size ($\Delta t = 10^{-6}$).

First, we are interested in the error (defined by (5.3)) against the number of grid points M for the quantities $\mathbf{x}(t)$, $\mathbf{v}_{\|}(t) := \mathbf{v}(t) \cdot \mathbf{B}(\mathbf{x}(t))\mathbf{B}(\mathbf{x}(t))/\|\mathbf{B}(\mathbf{x}(t))\|^2$ and $|\mathbf{v}(t)|$ at $T = 1$. In Figure 6, we can observe that the proposed MM scheme converges as the number of grid points M increases (Δs decreases) with a uniform second order accurate rate for all $\varepsilon]0, 1]$.

Then, in Figure 7, the time history of the energy error (defined by (5.4)) of the method with $\Delta s = 1/8$ and $\Delta s = 1/16$ until a physical time $T = T(s) = 100$ and under three different ε is shown. Let us remark that the restart strategy is used at every time step. In Figure 7, we observe that the scheme computes the energy (5.2) with uniform second order accuracy for $\varepsilon \in]0, 1]$. Under a rather large step size ($\Delta s \gg \varepsilon$), the scheme is stable in long time computing, and even if a slight linear drift in the energy error is observed, the energy error (about 10^{-3}) is rather good for all ε considered. In Figure 7, the relation between the new time s and the physical time $t(s)$ is also plotted to illustrate that the physical time $t(s)$ is a monotone increasing function.

Finally, we study the dynamics of the magnetic moment defined by

$$I(t) = \frac{1}{2} \frac{|\mathbf{v}_{\perp}(t)|^2}{|\mathbf{B}(\mathbf{x}(t))|}, \tag{5.5}$$

which is an analogy of (4.7) at the particle level (5.1). We use MM with $\Delta s = 1/16$ (so that it is accurate enough) to solve (5.1) until $t = 100$ with three different values of ε ($\varepsilon = 2^{-9}, 2^{-10}, 2^{-11}$). In Figure 8, the relative error on the magnetic moment, i.e., $|I(t_n) - I(0)|/(\varepsilon I(0))$, is displayed as a function of the rescaled time s. Let us remark that the MM scheme captures this quantity $I(t)$ with uniform second order accuracy for $\varepsilon \in]0, 1]$ since $I(t)$ only depends on $|\mathbf{v}|$ and $\mathbf{v}_{\|}$ through $|\mathbf{v}_{\perp}|^2 = |\mathbf{v}|^2 - |\mathbf{v}_{\|}|^2$. The deviation of the magnetic moment (5.5) behaves as $|I(t) - I(0)| = O(\varepsilon)$ in the simulation, which is consistent with the results obtained in [26]. Our scheme captures

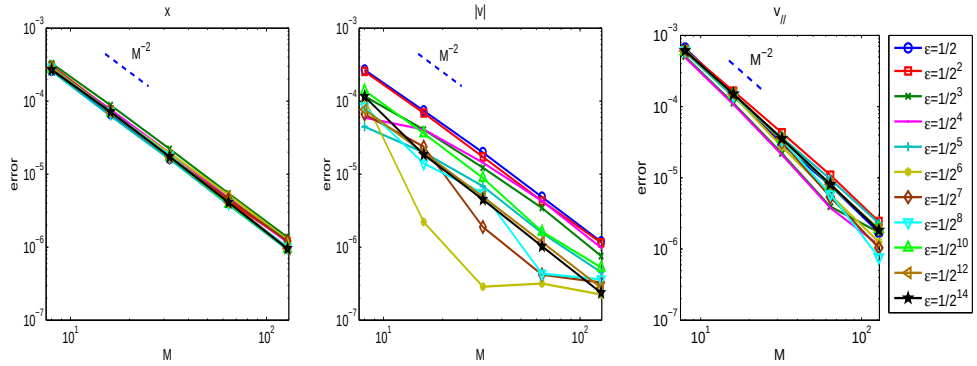

FIG. 6. *Error of MM under different* $M = \Delta s^{-1}$ *in* $\mathbf{x}$, $|\mathbf{v}|$, *and* $\mathbf{v}_{\|}$ *at* $T = 1$ *in Example* 5.2 *of varying intensity.*

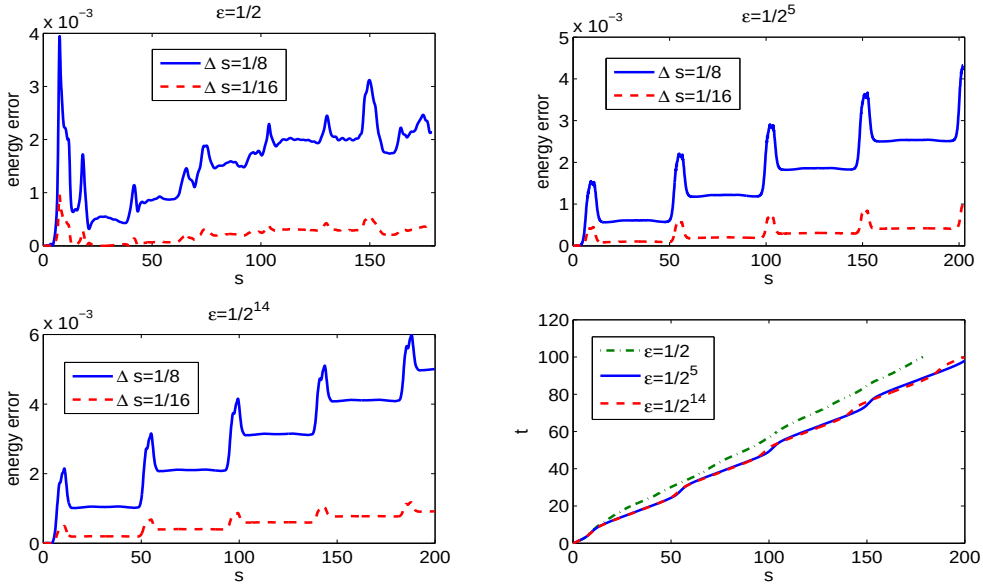

FIG. 7. *Energy error of MM (restart each step) for* $\varepsilon = 1/2, 1/2^5, 1/2^{14}$ *until* $t = 100$ *and the evolution of* $t(s)$ *in Example* 5.2.

this adiabatic quantity even when $\Delta s \gg \varepsilon$, whereas the scheme used in [26] needs $\Delta s < \varepsilon$.

5.2. Simulation of the Vlasov–Poisson system. In this last part, we focus on the numerical simulation of the full three dimensional Vlasov–Poisson equation (1.1) using the MRC method. The chosen initial data is a Maxwellian in velocity and a ring-shape distribution in space with a perturbation in angle [18]:

$$f_0(\mathbf{x}, \mathbf{v}) = \frac{n_0}{2\pi} \left(1 + \eta \cos(k\theta)\right) \mathrm{e}^{-5(r-5)^2} \mathrm{e}^{-\frac{1}{2}|\mathbf{v}|^2}, \tag{5.6}$$

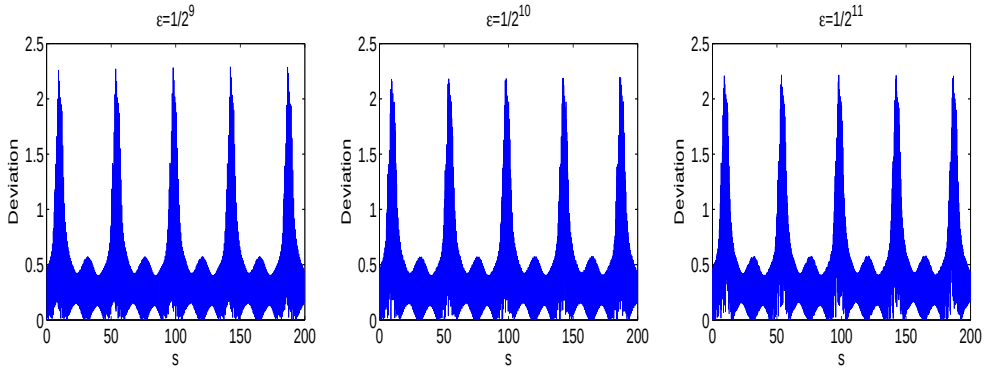

FIG. 8. *Deviation of the magnetic moment:* $\frac{1}{\varepsilon}|I(t) - I(0)|/I(0)$ *until* $t = 100$ *in Example* 5.2 *under different* ε *(computed with* $\Delta s = 1/16 \gg \varepsilon$*, ratios* $\Delta s/\varepsilon = 32, 64, 128$*).*

where $\mathbf{x} = (x_1, x_2, x_3)$, $\mathbf{v} = (v_1, v_2, v_3)$, $r = |\mathbf{x}|$, and $\theta = \arctan(x_2/x_1)$. The nonhomogeneous magnetic field is taken as in [30] (screw-pinch setup):

$$\mathbf{B}(\mathbf{x}) = \frac{1}{\sqrt{1 + \alpha^2 x_1^2 + \alpha^2 x_2^2}} \begin{pmatrix} \alpha x_2 \\ -\alpha x_1 \\ 1 \end{pmatrix},$$

which satisfies both $|\mathbf{B}(\mathbf{x})| = 1$ and $\nabla_{\mathbf{x}} \cdot \mathbf{B}(\mathbf{x}) = 0$. The spatial domain is a Cartesian geometry $\mathbf{x} = (x_1, x_2, x_3) \in \Omega = [-8, 8] \times [-8, 8] \times [0, 1]$. We choose $n_0 = 100$, $\eta = 0.05$, $k = 4$ and discretize the spatial domain Ω with $N_{x_1} = N_{x_2} = 256$ points in the x_1, x_2-directions and $N_{x_3} = 4$ points in the x_3-direction. As a diagnostic, we consider the following quantity:

$$\rho^\varepsilon(t, \mathbf{x}) = \int_{\mathbb{R}^3} f^\varepsilon(t, \mathbf{x}, \mathbf{v}) d\mathbf{v}, \qquad \mathbf{x} \in \Omega.$$

For the PIC method, we choose $N_p = 100 \times N_{x_1} N_{x_2} N_{x_3}$ particles and the projection of the particles on the spatial grid is done by cubic splines.

In Figure 9, the density ρ^ε is displayed at different times for $\varepsilon = 1/2^5$ with $M = 256$ in MRC until $t = 64\pi$ (so $M_0 = H/\varepsilon = 4$ in (3.5)), whereas $\alpha = 0$ in the magnetic field, so that $\mathbf{B}$ is homogeneous and aligned with the x_3-direction. There are two different dynamics which can be seen in the results: an instability develops in the direction orthogonal to the magnetic field (one can see four vortices at time $t = 64\pi$), and a slight parallel dynamics develops in the plane parallel to the magnetic field. In Figures 10 and 11, a nonhomogeneous magnetic field is considered ($\alpha = 0.003$). We can observe that the dynamics is different from the homogeneous case. Indeed, the instability leading to the formation of four vortices is different and one can see stronger nonhomogeneous phenomena in the x_3-direction due to the expression of the magnetic field.

Finally, in Figure 12, we plot the energy error for both configurations ($\alpha = 0$ and $\alpha = 0.003$). Very good conservations are obtained for long times. Moreover, we consider the relative error between the Vlasov–Poisson system (1.1) and the asymptotic model (2.4) as a function of ε for $\alpha = 0.003$. To do so, we compute the L^∞ norm (in space) of $|\rho^\varepsilon(t = \pi, \mathbf{x}) - \rho(t = \pi, \mathbf{x})|/|\rho^\varepsilon(t = \pi, \mathbf{x})|$ at the final time $t = \pi$. We can see that when ε decreases, the error is $O(\varepsilon)$, as predicted by the theory.

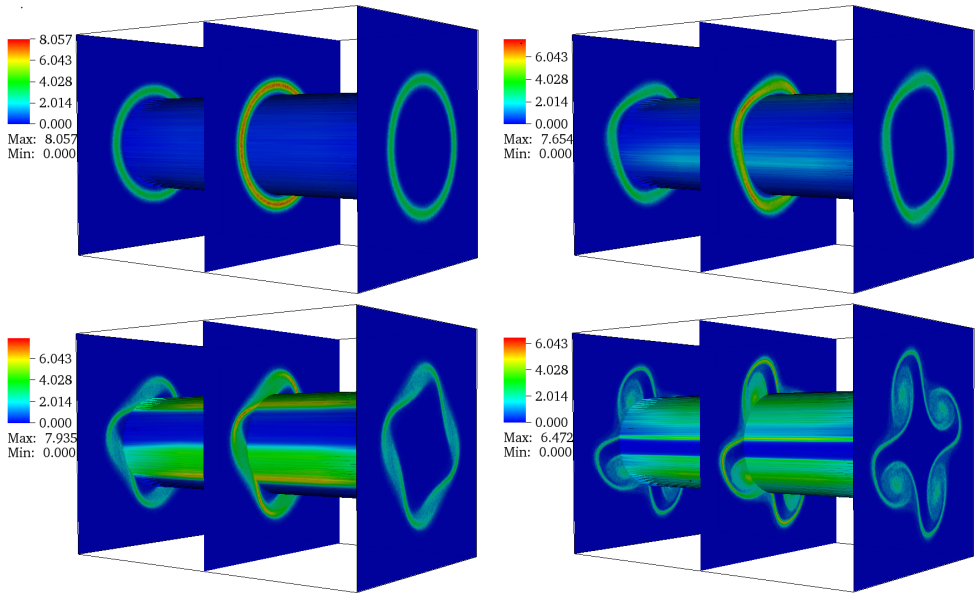

FIG. 9. *Vlasov–Poisson case: pseudocolor snapshots of* ρ^ε *under* $\varepsilon = 1/2^5$ *at* $t = 0, 16\pi, 32\pi, 64\pi$ *with initial condition* (5.6) *with* $\alpha = 0$.

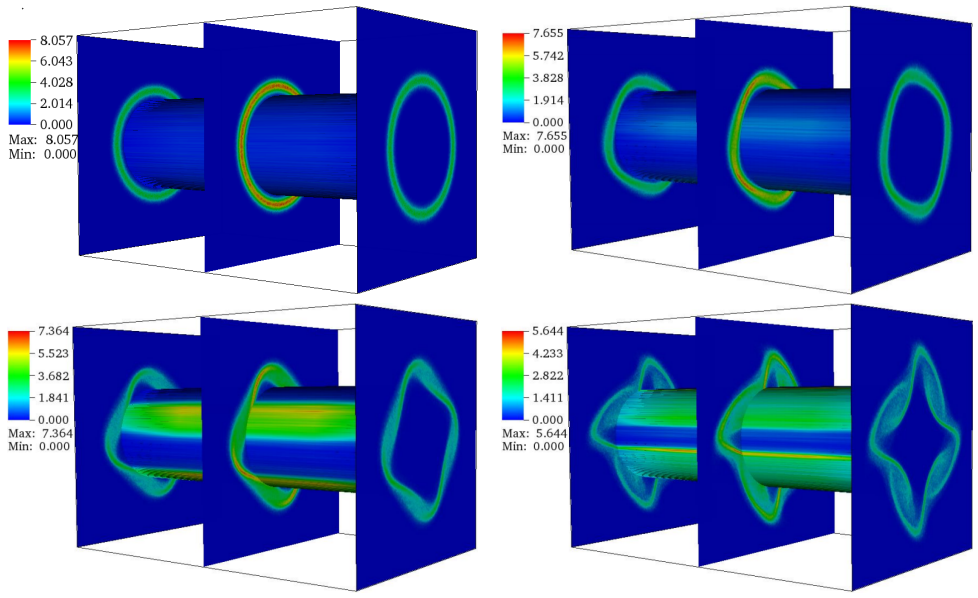

FIG. 10. *Vlasov–Poisson case: pseudocolor snapshots of* ρ^ε *under* $\varepsilon = 1/2^5$ *at* $t = 0, 16\pi, 32\pi, 64\pi$ *with initial condition* (5.6) *with* $\alpha = 0.003$.

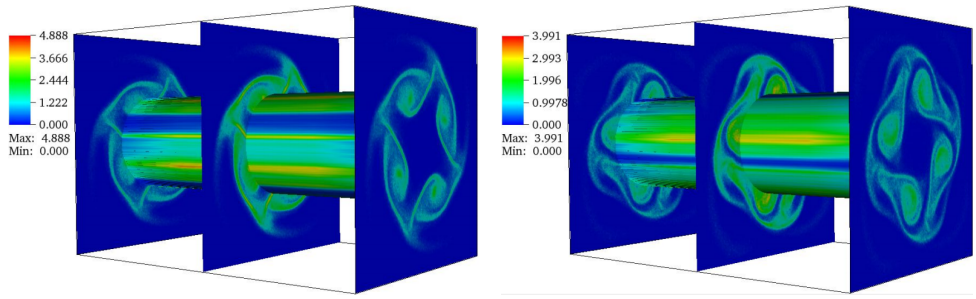

FIG. 11. *Vlasov–Poisson case: pseudocolor snapshots of* ρ^ε *under* $\varepsilon = 1/2^5$ *at* $t = 88\pi, 128\pi$ *with initial condition* (5.6) *with* $\alpha = 0.003$.

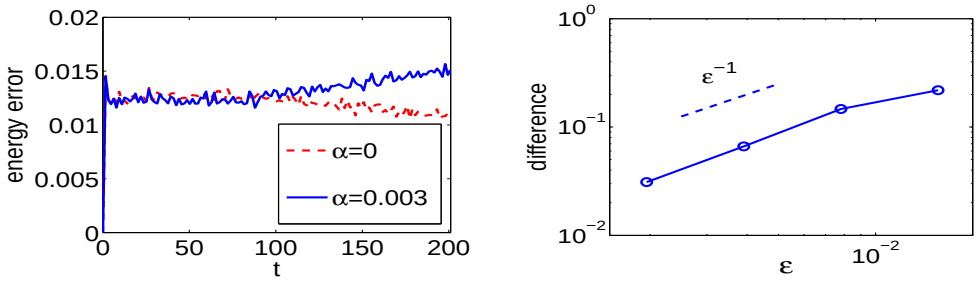

FIG. 12. *Vlasov–Poisson case. Left: time history of the energy error with initial condition* (5.6). *Right: difference between* (1.1) *and the limit model* (2.4) *(maximum error of* $|\rho^\varepsilon(t = \pi, \mathbf{x}) - \rho(t = \pi, \mathbf{x})|/|\rho^\varepsilon(t = \pi, \mathbf{x})|$*).*

REFERENCES

[1] A. ABDULLE, W. E, B. ENGQUIST, AND E. VANDEN-EIJNDEN, *The heterogeneous multiscale method*, Acta Numer., 21 (2012), pp. 1–87.

[2] C. K. BIRDSALL AND A. B. LANGDON, *Plasma Physics via Computer Simulation*, Adam Hilger, Bristol, UK, 1991.

[3] M. BOSTAN, *The Vlasov–Maxwell system with strong initial magnetic field: Guiding-center approximation*, Multiscale Model. Simul., 6 (2007), pp. 1026–1058, https://doi.org/10.1137/070689383.

[4] M. BOSTAN, *Gyrokinetic Vlasov equation in three dimensional setting. Second order approximation*, Multiscale Model. Simul., 8 (2010), pp. 1923–1957, https://doi.org/10.1137/090777621.

[5] M. BOSTAN AND A. FINOT, *The effective Vlasov–Poisson system for the finite Larmor radius regime*, Multiscale Model. Simul., 14 (2016), pp. 1238–1275, https://doi.org/10.1137/16M1060479.

[6] PH. CHARTIER, N. CROUSEILLES, AND M. LEMOU, *An Averaging Technique for Transport Equations*, preprint, https://arxiv.org/abs/1609.09819v1, 2018.

[7] PH. CHARTIER, N. CROUSEILLES, M. LEMOU, AND F. MÉHATS, *Uniformly accurate numerical schemes for highly oscillatory Klein-Gordon and nonlinear Schrödinger equations*, Numer. Math., 129 (2015), pp. 211–250.

[8] PH. CHARTIER, N. CROUSEILLES, M. LEMOU, F. MÉHATS, AND X. ZHAO, *Uniformly accurate methods for Vlasov equations with non-homogeneous strong magnetic field*, Math. Comp., 88 (2019) pp. 2697–2736.

[9] PH. CHARTIER, N. CROUSEILLES, AND X. ZHAO, *Numerical methods for the two-dimensional Vlasov-Poisson equation in the finite Larmor radius approximation regime*, J. Comput. Phys., 375 (2018), pp. 619–640.

[10] PH. CHARTIER, M. LEMOU, F. MÉHATS, AND G. VILMART, *A new class of uniformly accurate methods for highly oscillatory evolution equations*, Found. Comput. Math., 20 (2020),

pp. 1–33.
[11] Ph. Chartier, J. Makazaga, A. Murua, and G. Vilmart, *Multi-revolution composition methods for highly oscillatory differential equations*, Numer. Math., 128 (2014), pp. 167–192.
[12] Ph. Chartier, F. Méhats, M. Thalhammer, and Y. Zhang, *Convergence analysis of multi-revolution composition time-splitting pseudo-spectral methods for highly oscillatory differential equations of Schrödinger equations*, ESAIM Math. Model. Numer. Anal., 51 (2017), pp. 1859–1882.
[13] N. Crouseilles, S. A. Hirstoaga, and X. Zhao, *Multiscale Particle-in-Cell methods and comparisons for long time two-dimensional Vlasov-Poisson equation with strong magnetic field*, Comput. Phys. Commun., 222 (2018), pp. 136–151.
[14] N. Crouseilles, M. Lemou, and F. Méhats, *Asymptotic preserving schemes for highly oscillatory Vlasov-Poisson equations*, J. Comput. Phys., 248 (2013), pp. 287–308.
[15] N. Crouseilles, M. Lemou, F. Méhats, and X. Zhao, *Uniformly accurate forward semi-Lagrangian methods for highly oscillatory Vlasov–Poisson equations*, Multiscale Model. Simul., 15 (2017), pp. 723–744, https://doi.org/10.1137/16M1059497.
[16] N. Crouseilles, M. Lemou, F. Méhats, and X. Zhao, *Uniformly accurate particle-in-cell method for the long time two-dimensional Vlasov-Poisson equation with uniform strong magnetic field*, J. Comput. Phys., 346 (2017), pp. 172–190.
[17] P. Degond and F. Filbet, *On the asymptotic limit of the three dimensional Vlasov-Poisson system for large magnetic field: Formal derivation*, J. Stat. Phys., 65 (2016), pp. 765–784.
[18] F. Filbet and C. Yang, *Numerical Simulations to the Vlasov-Poisson System with a Strong Magnetic Field*, preprint, https://arxiv.org/abs/1805.10888, 2018.
[19] F. Filbet, T. Xiong, and E. Sonnendrücker, *On the Vlasov–Maxwell system with a strong magnetic field*, SIAM J. Appl. Math., 78 (2018), pp. 1030–1055, https://doi.org/10.1137/17M1112030.
[20] F. Filbet and L. M. Rodrigues, *Asymptotically stable particle-in-cell methods for the Vlasov-Poisson system with a strong external magnetic field*, SIAM J. Numer. Anal., 54 (2016), pp. 1120–1146, https://doi.org/10.1137/15M104952X.
[21] F. Filbet and L. M. Rodrigues, *Asymptotically preserving particle-in-cell methods for inhomogeneous strongly magnetized plasmas*, SIAM J. Numer. Anal., 55 (2017), pp. 2416–2443, https://doi.org/10.1137/17M1113229.
[22] E. Frénod, S. A. Hirstoaga, M. Lutz, and E. Sonnendrücker, *Long time behavior of an exponential integrator for a Vlasov-Poisson system with strong magnetic field*, Commun. Comput. Phys., 18 (2015), pp. 263–296.
[23] E. Frénod, F. Salvarani, and E. Sonnendrücker, *Long time simulation of a beam in a periodic focusing channel via a two-scale PIC-method*, Math. Models Methods Appl. Sci., 19 (2009), pp. 175–197.
[24] E. Frénod and E. Sonnendrücker, *Long time behavior of the two-dimensional Vlasov equation with a strong external magnetic field*, Math. Models Methods Appl. Sci., 10 (2000), pp. 539–553.
[25] F. Golse and L. Saint-Raymond, *The Vlasov-Poisson system with strong magnetic field*, J. Math. Pures Appl. (9), 78 (1999), pp. 791–817.
[26] E. Hairer and Ch. Lubich, *Long-term analysis of a variational integrator for charged-particle dynamics in a strong magnetic field*, Numer. Math., 144 (2020), pp. 699–728.
[27] G. B. Jacobs and J. S. Hesthaven, *Implicit-Explicit time integration of a high-order particle-in-cell method with hyperbolic divergence cleaning*, Comput. Phys. Comm., 180 (2009), pp. 1760–1767.
[28] S. Jin, *Efficient asymptotic-preserving (AP) schemes for some multiscale kinetic equations*, SIAM J. Sci. Comput., 21 (1999), pp. 441–454, https://doi.org/10.1137/S1064827598334599.
[29] M. Kraus, K. Kormann, P. Morrison, and E. Sonnendrücker, *GEMPIC: Geometric electromagnetic particle in cell methods*, J. Plasma Phys., 83 (2017), 905830401.
[30] G. Latu, M. Mehrenberger, Y. Güçlü, M. Ottaviani, and E. Sonnendrücker, *Field-aligned interpolation for semi-Lagrangian gyrokinetic simulations*, J. Sci. Comput., 74 (2018), pp. 1601–1650.
[31] W. W. Lee, *Gyrokinetic approach in particle simulation*, Phys. Fluids, 26 (1983), pp. 556–562.
[32] T. G. Northrop, *The Adiabatic Motion of Charged Particles. Interscience Tracts on Physics and Astronomy*, Vol. 21, Interscience/John Wiley & Sons, New York, London, Sydney, 1963.
[33] H. Qin, J. Liu, J. Xiao, R. Zhang, Y. He, Y. Wang, Y. Sun, J. W. Burby, L. Ellison, and Y. Zhou, *Canonical symplectic particle-in-cell method for long-term large-scale sim-*

ulations of the Vlasov-Maxwell system, Nucl. Fusion, 56 (2016), 014001.
[34] L. Saint-Raymond, *The gyro-kinetic approximation for the Vlasov-Poisson system*, Math. Models Methods Appl. Sci., 10 (2000), pp. 1305–1332.
[35] J. A. Sanders and F. Verhulst, *Averaging Methods in Nonlinear Dynamical Systems*, Appl. Math. Sci. 59, Springer-Verlag, New York, 1985.
[36] E. Sonnendrücker, *Numerical Methods for Vlasov Equations*, Lecture notes, 2016.